Vol. 91 No. 6 pp. 2058–2077 ACTA GEOLOGICA SINICA (English Edition) Dec. 2017

Indo–Chinese Magmatic Activity in the Duobaoshan District of Heilongjiang Province and Its Geological Significance

LI Yun[1, 2], HOU Xiaoyu[1], YANG Bo[1], ZHAO Yuanyi[2, *] and CHEN Long[1]

1 *China University of Geosciences, Beijing 100083, China*

2 *Key Laboratory of Metallogeny and Mineral Assessment of the Institute of Mineral Resources of Geological Sciences, Chinese Academy of Geological Sciences, Ministry of Land and Resources, Beijing 100037, China*

Abstract: The Duobaoshan ore concentration area, located in Nenjiang County of Heilongjiang Province, is an important porphyry Cu-Mo ore concentration area in China, which is characterized by complex magmatic activities and multi–phase overprinting metallogenesis. On the basis of field geological observation, systematic sampling, in-lab analysis and the metallogenic regularity in the Xiang'an–Mongolian metallogenic belt, this work carried out high-precision dating and geochemical analysis on the Yuejin, 173-kilometer and Wolihedingzi rock bodies. These rock bodies are renamed monzonitic granite and their consistent age (238 Ma) show that they were formed not in Variscan but in Indosinian. Therefore, it is inferred that the ore spots formed in the potassium silicate and sericite alteration zones of the rock mass also belong to Indosinian. In addition, we collected granodiorite from the Tongshan mining pit, and its zircon age is 223.1±2.8 Ma and the Cu content of the sample is high. The Tongshan mineralization is inferred to undergo the superimposition of Indosinian diagenetic mineralization. The age of the granodiorite porphyry related to copper-molybdenum mineralization in the Xiaoduobaoshan area is 222.1±5.5 Ma, and the earlier age of granodiorite is 471.8±7.4 Ma, indicating that the initial magmatic activities belong to the Duobaoshan porphyry system in the Caledonian period. The geochemical characteristics of the Indosinian rock samples show continental arc features, with reference to tectonic-magmatic activities of the whole Daxing'anling area. We consider that the magmatic activities and mineralization of the Indosinian period are affected by the southward subduction of Okhotsk Ocean since Late Permian. By combining the mineralization rules of Daxinganling area and the structural systems of Duobaoshan ore concentration area, we divide two rock-mineralization belts in this area including the Yuejin–Duobaoshan–Tongshan belt and 173-kilometer–Xiaoduobaoshan–Wolihedingzi belt, which are distributed nearly parallel along the NW-trending fractures and show similar geotectonic settings and the timing of the magmatic activities. It is favorable for discovering porphyry Cu-Mo deposits in these two metallogenic belts, especially in the Yuejin, 173-kilometer and Wolihedingzi areas where less research work has been made.

Key words: Indosinian, Okhotst Ocean, prospecting direction, Duobaoshan, Heilongjiang Province

1 Introduction

The Duobaoshan ore concentration area located in Nenjiang County, Heilongjiang Province contains abundant mineral resources. Since the discovery of the Duobaoshan porphyry Cu deposit in 1958, a total of 14 metallic deposits (occurrences) have been discovered successively from Sankuanggou in the northwest to the Daye (Zhao Guangjiang et al., 2006), among which the accumulative proven reserves of the Duobaoshan deposit and Tongshan deposits 4 km to the southwest include 3.35 million tons of Cu, 0.15 million tons of Mo and 0.73 million tons of Au (Du Qi et al., 1998), both belonging to large deposits. The magmatic activities in the area exhibit the features of multi-phase overprinting magmatic activities. The diagenetic and metallogenic ages determined previously (Table 1) concentrate in Caledonian (474−526 Ma), Variscan (256−310 Ma) and Yanshanian

* Corresponding author. E-mail: yuanyizhao2@sina.com

Table 1 Results of diagenesis and mineralization in the Duobaoshan ore deposit (from northwest to southeast)

Name of rock body	Samples and test methods	Age (Ma)	Data source
Highway Nenmo184-kilometers	Biotite K-Ar age of granodiorite	181.4 or 180.8	ZhaoYiming, 1997
Highway Nenmo156-kilometers	Biotite K-Ar age of oblique lamprophyre	245	Li Derong, 2010
Sankuanggou	Zircon U-Pb age of granodiorite	209	Li Derong, 2010
	Biotite K-Ar age of granodiorite	180.8–201	Li Derong, 2010
	K-Ar age of granodiorite	184	Li Derong, 2010
	K-Ar age of tonalite	172	Li Derong, 2010
	SHRIMP Zircon U-Pb age of tonalite	177	Li Derong, 2010
	Zircon U-Pb age of tonalite	200±1	Lv Pengrui, 2012
	U - Pb weighted average age of the SHRIMP zircons from the hornblende biotite granodiorite	177±3	Ge Wenchun, 2007
	U - Pb weighted average age of the SHRIMP zircons from the biotite granodiorite	176±3	Ge Wenchun, 2007
	Zircon U-Pb age of granodiorite	175.9±1.6	Chu Shaoxiong, 2012
	Weighted mean zircon age of granodiorite	175.9±1.1	Chu Shaoxiong, 2012
	Zircon U-Pb age of granodiorite	173.4±1.0	Our project team
Yubaoshan	U-Pb age of serpentinized pyroxenite	526.6±7.3	Our project team
173-kilometers	Biotite K-Ar age of quartz diorite	170.7	Zhao Yiming, 1997
	Zircon U-Pb age of monzonitic granite	238.5±2.1	Our project team
Wulicha	K-Ar age of biotite in monzonitic granite	223	Zhao Yiming, 1997
Luohe	Biotite K-Ar age of granodiorite	109.9	Zhao Yiming, 1997
	K-Ar age of quartz diorite	182	Li Derong, 2010
	Zircon U-Pb age of granodiorite	174.0±2.1	Our project team
Xiaoduobaoshan	Zircon U-Pb age of granodiorite porphyry	222.1±5.5	Our project team
Jiguanshan	K-Ar age of granodiorite	234	Zhao Yiming, 1997
	Zircon U-Pb age of granodiorite	312.8±2.6	Our project team
Yuejin	Biotite K-Ar age of granodiorite	291.5	Zhao Yiming, 1997
	Diorite and granite K-Ar age	234–249	Li Derong, 2010
	U-Pb age of monzonitic granite	238.1±2.4	Our project team
Wolihedingzi	K-Ar age of granodiorite	249 or 239	Zhao Yiming, 1997
	K-Ar age of K-feldspar vein	236	Li Derong, 2010
	monzonitic granite	238.4±2.0	Our project team
Duobaoshan	Molybdenite Re-Os age	521±20	Zhao Yiming, 1997
	Molybdenite Re-Os age	509±5	Zhao Yiming, 1997
	Molybdenite Re-Os age	507±3	Zhao Yiming, 1997
	Chalcopyrite Re-Os isochron	481.9±6.7	Liu Jun, 2012
	Chalcopyrite Re-Os isochron	484.9±7.3	Liu Jun, 2012
	Molybdenite Re-Os age	485.6±3.7	Liu Jun, 2012
	Alteration granodiorite molybdenum isochron	506±14	Cui Gen, 2008
	SHRIMP zircon U - Pb weighted average age of granodiorite	479.5±4.6	Cui Gen, 2008
	SHRIMP zircon U - Pb weighted average age of granodiorite	479.5±4.6	Zhao Huanli, 2012
	U-Pb age of granodiorite porphyry	485.6±3.7	Xiang Anping, 2012
	Zircon U - Pb age of granodiorite	478.1±4.1	Xiang Anping, 2012
	U-Pb age of biotite granodiorite	483.9±4.5	Xiang Anping, 2012
	Molybdenite Re-Os age	475.1±5.1	Xiang Anping, 2012
	Granodiorite Rb-Sr isochron	310±17	Li Derong, 2010
	K-Ar age of granodiorite	292	Li Derong, 2010
	K-Ar age of granodiorite porphyry	283	Li Derong, 2010
	U-Pb age of granodiorite porphyry	485.6±3.7	Our project team
	K-Ar age of granodiorite	475.9±3.5	Our project team
	U-Pb age of tonalite	479.6±3.7，230.9±2.8Ma	Our project team
Tongshan	K-Ar age of granodiorite	256.3–292	Zhao Yiming, 1997a
	^{40}Ar-^{39}Ar age of sericite in silicified granodiorite	252.5	Zhao Yiming, 1997a
	Molybdenite Re-Os isochron	476±14	Zhao Yiming, 1997a
	Molybdenite Re-Os isochron	505±14	Zhao Yiming, 1997a
	Molybdenite Re-Os isochron	506±14	Cui Gen, 2008
	U-Pb age of granite porphyry	230.9±0.9	Hao YuJie, 2015
	U-Pb age of granodiorite	223.1±2.8	Our project team
Zhengguang	K-Ar age of the diorite quartz diorite	182Ma	Li Derong, 2010
	^{40}Ar-^{39}Ar age of dioritic alteration minerals	172.5–178.1	Li Derong, 2010
	Molybdenite Re-Os isochron	480±3	Our project team
	U-Pb age of diorite	478.3±3.7	Our project team
	^{40}Ar-^{39}Ar age of diatomite sericite	188.8±1.3	Our project team
	U-Pb age of diorite	150.6±0.77	Our project team

(156−209 Ma) (Zhao Yiming., 1997a; Wang Xicheng et al., 2007; Cui Gen et al., 2008), which are consistent with the main diagenetic and metallogenic ages of the Great Xing'an Range region (She Hongquan et al., 2012).

However, we yielded the ages of these rock bodies by high-precision LA-ICP-MS zircon method varying from 223 Ma to 238 Ma, belonging to Indosinian. Therefore, we believe that the deposits in the Yuejin and Xiaoduobaoshan areas were formed not in Variscan but in Indosinian. In addition, based on further study of the samples in Tongshan, it is suggested that the important metallogenesis also occurred in Indosinian. In order to further study the Indosinian diagenesis and metallogenesis in the study area, on the basis of field geological observation, systematic sampling and in-lab analysis, and combining with the metallogenic regularity in the Great Xing'an Range region, this work discussed the diagenetic and metallogenic ages in the Yuejin and Xiaoduobaoshan areas as well as the characteristics of the multi-phase magmatic activities in order to fill in the gap of the Indosinian magmatic activities and prospecting in the region(Mao Zhiguo et al., 2015; Yang Yongqiang et al., 2016), and promote further prospecting in the 173-kilometer and Wolihedingzi rock bodies.

2 Geological Settings

2.1 Regional geological settings

The Duobaoshan ore concentration area is situated in the east of the Central Asian–Mongolian porphyry copper belt, and the northeastern border region between the Inner Mongolian–Great Xing'an Range fold system and the Jilin–Heilongjiang fold system. In terms of tectonic units, the ore concentration is attributed to the Xing'an block, which is bounded by the Tayuan–Xiguitu fault in the Erguna block in the northwest and by the Nenjiang fault in the Songnen block in the southeast. Within this ore concentration covering an area of 420 km^2 from Sankuanggou in the northwest to Zhengguang in the southeast (Zhao Yuanyi et al., 2011), the Sankuanggou skarn Cu-Fe deposit, Yubaoshan skarn Cu-Fe deposit, Yuejin–Jiguanshan porphyry Mo-Cu occurrence(Xing Shuwen et al., 2016), Duobaoshan porphyry Cu-Mo deposit, Tongshan porphyry Cu-Mo deposit and Zhengguang epithermal gold deposit have been discovered. These deposits (occurrences) are distributed mainly in a NW-trending arcuate tectonic belt (Fig. 1). The Duobaoshan arcuate tectonic belt converges with the Duobaoshan overturned anticline axial zone and a number of structures in the Duobaoshan ore district (Fig. 1), and relatively significant ore-controlling structures are the NW-trending arcuate structures and the nearly EW-trending structures. The regional tectonic line of the Great Xing'an Range uplift belt is NE-trending, while the tectonic line in the ore field is NW-trending, nearly orthogonal to each other.

The strata known with outcrops of deposits (occurrences) in the ore field are dominated by Jurassic and Silurian systems. The main ore-hosting strata are the Middle–Ordovician Duobaoshan Formation (O_2d), which is set of volcanic rocks consisting of andesite and acid–intermediate tuff. The hydrothermal activities exhibit multi-phase overprinting features. They have closely spatial and temporal links with the magmatic activities of granodiorite, granodiorite porphyry and plagioclase granite.

2.2 Deposit (occurrence) characteristics

The Tongshan deposit is situated in the southeast of the Duoboashan deposit and the main stratum is the Duobaoshan Formation. The Caledonian granodiorite which is related to mineralization distribute widely (Zhao Yuanyi and Ma Zhihong, 1997a; Du Qi et al., 1998; Liu Jun et al., 2010; Wei Hao et al., 2011) and the Indosinian granodiorite has been discovered in the Tongshan ore district (Hao et al., 2015). The ore bodies are banded and lenticular, with thickness varying from several to tens of meters. In the Tongshan ore district, the average Cu grade is 0.44wt%, and the average Mo grade is 0.023wt%.

The Xiaoduobaoshan Cu-Mo deposit is situated in the northern part of the Duobaoshan deposit. The stratum exposed in the ore district is the Duobaoshan Formation (O_2d). The magmatic rock type is granodiorite porphyry. The rock bodies are distributed as NE–SW-trending narrow long bands, which are ~2.5 km long and ~500 m wide (Zhao Yiming et al., 1997b; Zhao Yuanyi et al., 1997b). The rock bodies are covered by thick vegetation, and can be seen only in trenches. The orebodies occur mainly in the internal and external contact zones between granodiorite porphyry and the Duobaoshan Formation (O_2d), and are often present in the Duobaoshan Formation. The orebodies occur as NW 320°–striking small lenses (Wu Guang et al., 2009), with average Cu grade of 0.4wt% and average Mo grade of 0.012wt% (Zhao Yuanyi et al., 2011). The orebodies are small in scale, with Cu content of 7100 t and Mo content of 154 t (Zhao Yiming et al., 1997b).

The Yuejin ore occurrence is located in the northwest of the Duobaoshan deposit. The strata where the ore occurrence is exposed are the Duobaoshan Formation. The magmatic rock type is granodiorite that occurs as overall NW 300°–trending stocks, with an area of ~0.6 km^2 (Wu Guang et al., 2009). There is thick overburden on the earth's surface. The orebodies occur as lenses, and the Mo mineralization is stronger than the Cu mineralization. The mineralization is present in the K-silicatization and phyllic ateration zones in the porphyraceous monzonitic granite. The rest two alteration zones are narrow and exhibit the

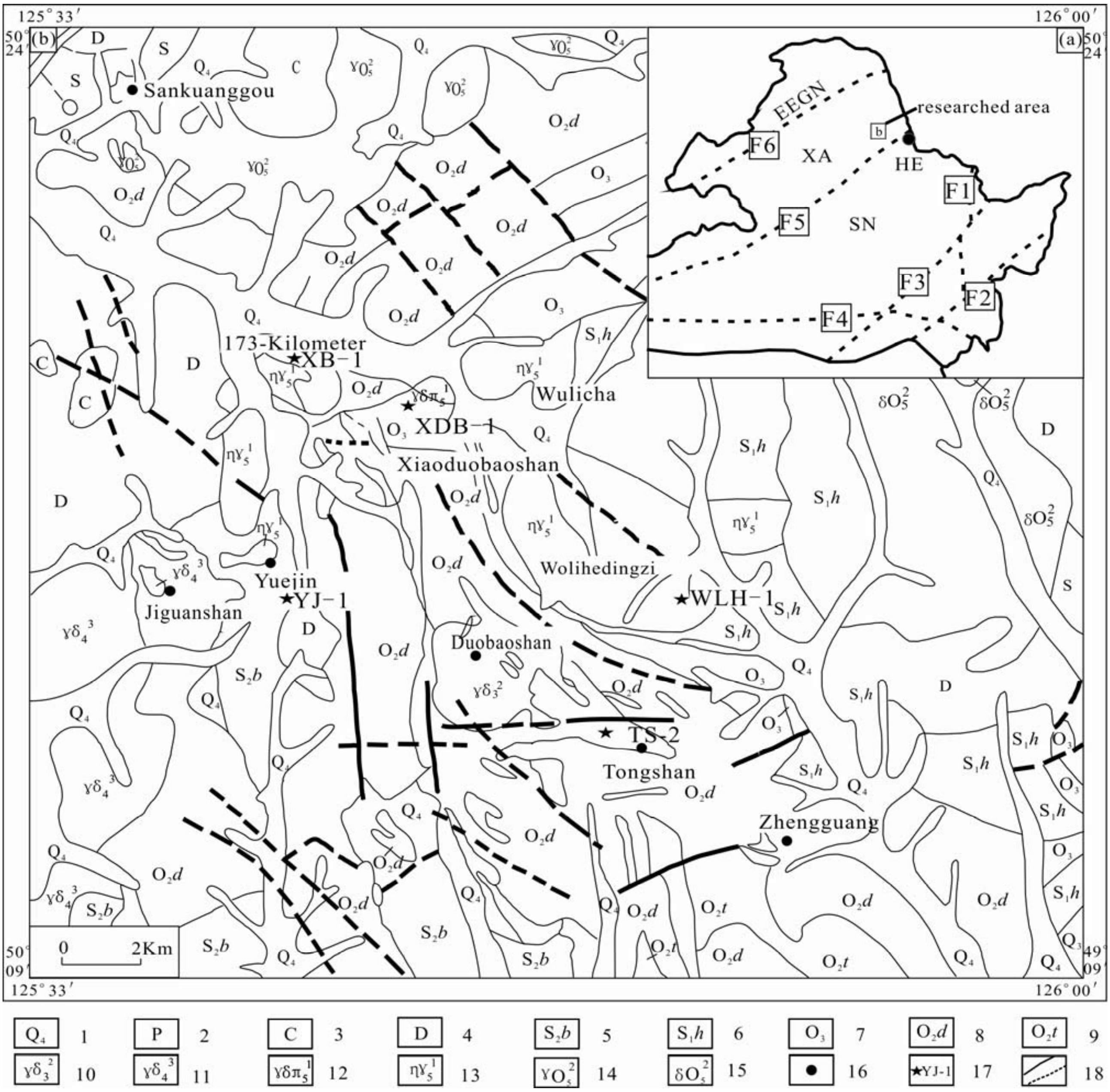

Fig. 1. (a), Map showing location of the deposit cluster; (b), Geological sketch map of the Duobaoshan deposit cluster (Yao Zhiqiang et al., 1995).

1, Quaternary; 2, Triassic; 3, Carboniferous; 4, Devonian; 5, 80-kilometer Xiaohe Fm.; 6, Lower Silurian Huanghuagou Fm; 7, Upper Ordovician; 8, Middle-Ordovician Duobaoshan Fm.; 9, Middle-Ordovician Tongshan Fm.; 10, Caledonian granodiorite; 11, Hercynian plagiogranite; 12, Indosinian granodiorite porphyry; 13, Indosinian monzogranite; 14, Yanshanian granodiorite; 15, Yanshanian quartz diorite; 16, Deposit (plot); 17, Sampling position and number; 18, Inferred/measured fault; EEGN, Erguna block; XA, Xing'an block; SN, Songnen block; HE, Heihe; F1, Mudanjiang fault; F2, Dunhua-Mishan fault; F3, Yitong-Yilan fault; F4, Xilamulun-Changchun fault; F5, Nenjing fault; F6, Tayuan-Xiguitu fault.

features of the roots of Cu and Mo deposits, with average Cu grade of 0.22wt%–0.59wt% and average Mo grade of 0.036wt%–0.072wt% (Yao Zhiqiang et al., 1995).

2.3 Orebody characteristics

The 173-kilometer rock body is located in the northwest part of the Xiaoduobaoshan deposit. The exposed stratum is the Duobaoshan Formation (O_2d). The rock body is dominated by granodiorite. The 173-kilometer rock body is EW-trending, and is controlled by an EW-trending fault. The Wolihedingzi rock body is located in the southeast part of the Xiaoduobaoshan deposit, and the exposed strata around it are the Duobaoshan (O_2d) and Huanghuagou (S_1h) formations. The dominant magmatic rock is granodiorite. The rock body is covered by thick vegetation, and almost no outcrop is found. It has been highly weathered into fragments, and alaskite veins are distributed around it, so it is difficult to trace and obtain the specific scale and occurrence of the rock body. It can be seen that a small amount of mineralization is produced in the potassium silicate and sericite alteration zones of the porphyritic monzonitic granite with the characteristics of the root belt of the porphyry copper-molybdenum deposit (Wu Taotao et al., 2016).

3 Sample Collection, Test and Results

3.1 Sample collection and characteristics

Because of thick overburden, samples in the Yuejin rock body were collected in a trench at 50˚14'58"N and 125˚39'38"E, with the sample numbers of YJ–1–1, YJ–1–2, YJ–1–3, YJ–1–7 and YJ–1–10. In the 173-kilometer rock body, the samples were collected in the location at 50˚18'46"N and 125˚39'52"E, with the sample numbers of XB–1–1, XB–1–2, XB–1–5, XB–1–6 and XB–1–7. Because of thick overburden, samples in the Wolihedingzi rock body were collected in a trench at 50˚15'01"N and 125˚49'49"E, with the sample numbers of WLH–1–8, WLH–1–9, WLH–1–10, WLH–1–11 and WLH–1–14. In the Tongshan rock body the samples were collected mainly near the highway entrance of Tongshan mining pit at 50˚12'54"N and 125˚47'58"E, with the sample numbers of TS–02–2, TS–02–3, TS–02–4, TS–02–5 and TS–02–6. Because of thick overburden, samples in the Xiaoduobaoshan rock body were collected in a trench at 50˚18'04"N and 125˚42'49"E, with the sample numbers of XDB–1–1, XDB–1–4, XDB–1–5, XDB–1–6 and XDB–1–7. These samples were collected using grappling method.

The monzonitic granite (YJ–1–10, Figs. 2a and 2b) from the Yuejin rock body, monzonitic granite (XB–1–1, Figs. 2c and 2d) from the 173-kilometer rock body, monzonitic granite (WLH–1–11, Figs. 2e and 2f) from the Wolihedingzi rock body are grey in color, and exhibit subhedral granular texture and massive structure. The quartz (accounting for 25vol.%−35vol.%) is xenomorphic granular, with grain sizes varying from 0.1 mm to 1.5 mm. The plagioclase (accounting for 30vol.%−40vol.%) is euhedral–subhedral and long columnar, with clear cleavages, and exhibits polysynthetic twinning, carlsbad–albite compound twin and zoning texture, with grain size of 0.4−1.5 mm. The K-feldspar (accounting for 25vol.%−35vol.%) is euhedral–subhedral and long columnar, and exhibits carlsbad twin, with grain sizes varying from 0.4 mm to 1.5 mm. The amphibolite (accounting for 1vol.%−2vol.%) is subhedral–xenomorphic and columnar, with carlsbad twin and grain sizes of 0.5−0.7 mm, and exhibits the metasomatism of amphibolited by pyrite. The biotite (accounting for 3vol.%−7vol.%) is flaky, with clear cleavages and median relief, with grain sizes between 0.4 mm and 0.8 mm. The muscovite (accounting for 3vol.%−5vol.%) is flaky, and exhibits clear cleavages, with grain sizes dominantly varying from 0.05 mm to 0.5 mm. The sericite (accounting for 3vol.%−5vol.%) occurs as small scales.

The granodiorite (TS–02–4, Figs. 2g and 2h) from the Tongshan rock body is grey in color, and exhibits subhedral granular texture and massive structure. The quartz (accounting for 20vol.%−25vol.%) is xenomorphic, with grain sizes varying from 0.15 mm to 2.0 mm. The plagioclase (accounting for 30vol.%−35vol.%) is euhedral–subhedral and columnar, with clear cleavages, and exhibits polysynthetic twinning, carlsbad–albite compound twin and zoning texture, with grain sizes varying from 0.2 mm to 2.0 mm. The K-feldspar (accounting for 10vol.%−15vol.%) is euhedral–subhedral and long columnar, and exhibits carlsbad twin, with grain sizes between 0.2 mm and 2.0 mm. The amphibolite (accounting for 2vol.%−3vol.%) is subhedral–xenomorphic and columnar, with grain sizes varying from 0.1 mm to 0.2 mm. The biotite (accounting for 3vol.%−5vol.%) is flaky, with clear cleavages and grain sizes varying from 0.1 mm to 0.25 mm. The sericite (accounting for 8vol.%−10vol.%) occurs as small scales, with grain sizes varying from 0.05 mm to 0.25 mm. The calcite (accounting for 2vol.%−3vol.%) exhibits rhomb cleavages. The chlorite (accounting for 2vol.%−3vol.%) exhibits indigo blue and rust brown abnormal interference color.

The granodiorite porphyry (XDB–1–4, Figs. 2i and 2j) from the Xiaoduobaoshan rock body is dark grey, and exhibits porphyritic texture and massive structure, in which phenocrysts account for 8vol.%−10vol.%, and matrix accounts for 85vol.%−90vol.%. The phenocrysts are dominated by amphibolite (0.2−0.7 mm in grain size) and plagioclase (0.8−1.5 mm in grain size). The matrix consists mainly of quartz, plagioclase, K–feldspar, biotite and minor chlorite, with grain size <0.15 mm.

3.2 Test and analytical methods

3.2.1 Zircon U–Pb chronological test and analysis

The LA-ICP-MS zircon target preparation and cathodoluminescence (CL) image analysis were undertaken at the Beijing GeoAnalysis Co., Ltd., and the relevant tests were undertaken at the LA-ICP-MS Micro Analysis Office of the Key Laboratory of Crust–Mantle Materials and Environments, University of Science and Technology of China, Chinese Academy of Sciences. The common lead was corrected using ComPb corr#3–18 (Anderson, 2002). The U-Pb concordia plots and the weighted mean age were calculated using Isoplot (Ludwig, 2003). ^{238}U and ^{235}U decay constants are 1.55125×10^{-10} a^{-1} and 9.8454×10^{-10} a^{-1}, respectively. The test results are

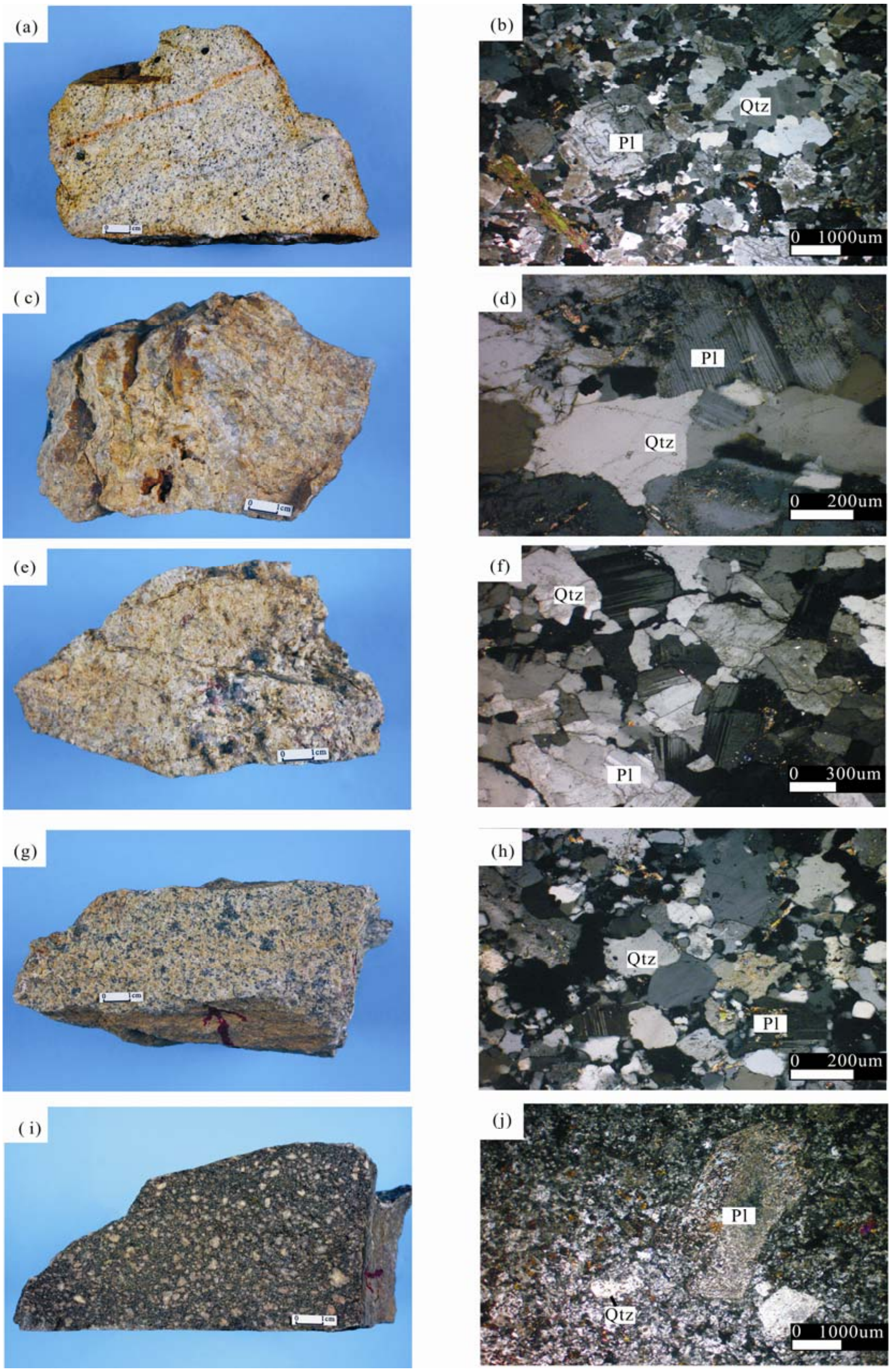

Fig. 2. Specimens and their microscopic photos.
(a), Monzonitic granite from the Yuejing rock body (YJ-1-10); (b), Monzonitic granite from the Yuejing rock body (under microscope); (c), Monzonitic granite from the 173-kilometer rock body (XB-1-1); (d), Monzonitic granite from the 173-kilometer rock body (under microscope); (e), Monzonitic granite from the Wolihedingzi rock body (WLH-1-11); (f), Monzonitic granite from the Wolihedingzi rock body (under the microscope); (g), Granodiorite from the Tongshan rock body (TS-02-4); (h), Granodiorite from the Tongshan rock body (under microscope); (i), Granodiorite porphyry from the Xiaoduobaoshan rock body (XDB-1-4); (j), Granodiorite porphyry from the Xiaoduobaoshan rock body (under the microscope).

Table 2 Statistic results of LA-ICP-MA zircon U-Pb ages of the rock bodies

Location	No.	ω(B)/(ppm)		Th/U	Isotopic ratio						Age/(Ma)					
		Th	U		$^{207}Pb/^{206}Pb$	1σ	$^{207}Pb/^{235}U$	1σ	$^{206}Pb/^{238}U$	1σ	$^{207}Pb/^{206}Pb$	1σ	$^{207}Pb/^{235}U$	1σ	$^{206}Pb/^{238}U$	1σ
Yuejin	YJ-1-1.01	135.11	205.55	0.66	0.05054	0.0033	0.27788	0.01693	0.03988	0.00099	220	146	249	13	252	6
	YJ-1-1.02	200.42	252.43	0.79	0.05201	0.00333	0.26545	0.01577	0.03702	0.0009	286	143	239	13	234	6
	YJ-1-1.03	78.44	145.95	0.54	0.0529	0.00398	0.27694	0.0194	0.03797	0.00097	324	168	248	15	240	6
	YJ-1-1.04	508.14	388.88	1.31	0.04825	0.00238	0.23415	0.01270	0.03520	0.00080	111	121	214	10	223	5
	YJ-1-1.05	150.05	210.25	0.71	0.0513	0.00317	0.26646	0.01537	0.03767	0.00093	254	132	240	12	238	6
	YJ-1-1.06	213.08	287.20	0.74	0.04995	0.00325	0.25207	0.01527	0.0366	0.00087	193	137	228	12	232	5
	YJ-1-1.07	81.95	155.86	0.53	0.04539	0.00386	0.22779	0.01833	0.0364	0.00095	-34	155	208	15	230	6
	YJ-1-1.08	178.23	243.04	0.73	0.0512	0.00337	0.27453	0.01649	0.03889	0.00095	250	148	246	13	246	6
	YJ-1-1.09	79.13	164.58	0.48	0.05403	0.00398	0.27881	0.01874	0.03743	0.00099	372	164	250	15	237	6
	YJ-1-1.10	70.56	146.45	0.48	0.05419	0.0045	0.26921	0.02132	0.03603	0.00106	379	172	242	17	228	7
	YJ-1-1.11	168.22	240.22	0.70	0.04992	0.00326	0.25162	0.01522	0.03656	0.00088	191	136	228	12	231	5
	YJ-1-1.12	165.08	224.54	0.74	0.05078	0.00331	0.26515	0.01621	0.03787	0.00093	231	139	239	13	240	6
	YJ-1-1.13	190.45	252.66	0.75	0.05057	0.00319	0.26034	0.01529	0.03734	0.0009	221	135	235	12	236	6
	YJ-1-1.14	90.98	181.46	0.50	0.05141	0.00355	0.26567	0.01704	0.03748	0.00096	259	157	239	14	237	6
	YJ-1-1.15	167.08	332.75	0.50	0.05320	0.00252	0.37957	0.02044	0.05174	0.00133	337	129	327	15	325	8
	YJ-1-1.16	188.68	196.97	0.96	0.04746	0.00367	0.24163	0.01735	0.03693	0.00093	72	160	220	14	234	6
	YJ-1-1.17	99.08	170.85	0.58	0.04985	0.00356	0.26461	0.01741	0.0385	0.00099	188	152	238	14	244	6
	YJ-1-1.18	85.23	163.09	0.52	0.05347	0.00367	0.27753	0.0177	0.03765	0.00095	349	140	249	14	238	6
	YJ-1-1.19	124.74	209.59	0.60	0.0486	0.00317	0.24926	0.01507	0.0372	0.00093	129	129	226	12	235	6
	YJ-1-1.20	169.51	220.30	0.77	0.04886	0.0031	0.25415	0.01544	0.03773	0.00093	141	137	230	12	239	6
	YJ-1-1.21	68.43	134.47	0.51	0.05318	0.00348	0.29413	0.02068	0.04011	0.00103	336	164	262	16	254	6
	YJ-1-1.22	105.74	179.30	0.59	0.05098	0.00404	0.26922	0.01905	0.0383	0.001	240	169	242	15	242	6
	YJ-1-1.23	56.93	122.13	0.47	0.04111	0.00409	0.22206	0.02008	0.03918	0.00109	-226	162	204	17	248	7
	YJ-1-1.24	164.04	231.48	0.71	0.04954	0.00301	0.26772	0.01539	0.03919	0.00097	174	139	241	12	248	6
	YJ-1-1.25	152.24	210.97	0.72	0.05264	0.00368	0.2689	0.01756	0.03705	0.00093	313	163	242	14	235	6
	YJ-1-1.26	60.25	149.74	0.40	0.0519	0.00395	0.27596	0.01932	0.03857	0.001	281	176	247	15	244	6
	YJ-1-1.27	234.58	243.34	0.96	0.03657	0.00266	0.19427	0.01354	0.03853	0.00092	-11	219	180	12	244	6
	YJ-1-1.28	253.02	289.36	0.87	0.0487	0.0031	0.24059	0.01425	0.03583	0.00087	133	132	219	12	227	5
	YJ-1-1.29	132.31	192.12	0.69	0.04728	0.00326	0.24694	0.01591	0.03788	0.00095	63	140	224	13	240	6
	YJ-1-1.30	133.65	204.00	0.66	0.05348	0.00368	0.27189	0.01733	0.03687	0.00091	349	144	244	14	233	6
	YJ-1-1.31	120.45	199.83	0.60	0.04933	0.00342	0.25628	0.01652	0.03768	0.00093	163	148	232	13	238	6
	YJ-1-1.32	64.55	122.16	0.53	0.05881	0.0045	0.31971	0.02371	0.03943	0.00105	560	164	282	18	249	7
173 kilometer	XB-1-2.01	49.59	155.76	0.32	0.05783	0.00244	0.59650	0.02884	0.07481	0.00178	523	93	475	18	465	11
	XB-1-2.02	59.21	127.85	0.46	0.04727	0.00306	0.24602	0.01672	0.03775	0.00096	63	137	223	14	239	6
	XB-1-2.03	170.33	213.76	0.80	0.04816	0.00237	0.25116	0.01338	0.03783	0.00089	107	104	228	11	239	6
	XB-1-2.04	126.64	184.56	0.69	0.05285	0.00285	0.28341	0.01634	0.0389	0.00095	322	120	253	13	246	6
	XB-1-2.05	182.45	241.43	0.76	0.05141	0.00226	0.27446	0.01362	0.03872	0.00092	259	94	246	11	245	6
	XB-1-2.06	87.90	135.65	0.65	0.05535	0.00339	0.27251	0.01739	0.03571	0.00092	427	127	245	14	226	6
	XB-1-2.07	224.45	507.62	0.44	0.05608	0.00185	0.52044	0.02055	0.06731	0.00147	455	69	425	14	420	9
	XB-1-2.08	267.39	314.79	0.85	0.05503	0.00239	0.28023	0.01369	0.03694	0.00087	413	94	251	11	234	5
	XB-1-2.09	29.29	77.14	0.38	0.06791	0.00852	0.35657	0.03809	0.03808	0.00122	866	261	310	29	241	8
	XB-1-2.10	66.18	125.48	0.53	0.07574	0.00337	0.79076	0.03999	0.07572	0.00182	1088	89	592	23	471	11
	XB-1-2.11	110.32	177.41	0.62	0.04905	0.00283	0.25333	0.01519	0.03746	0.00094	150	133	229	12	237	6
	XB-1-2.12	211.49	263.41	0.80	0.04898	0.00249	0.25539	0.01374	0.03782	0.00088	147	118	231	11	239	5
	XB-1-2.13	76.92	131.86	0.58	0.05171	0.0037	0.27418	0.02009	0.03846	0.00105	273	162	246	16	243	7
	XB-1-2.14	148.22	218.50	0.68	0.0513	0.00257	0.25875	0.01417	0.03658	0.0009	254	114	234	11	232	6
	XB-1-2.15	165.39	231.49	0.71	0.0528	0.00272	0.26451	0.01455	0.03633	0.00088	320	115	238	12	230	5
	XB-1-2.16	201.13	234.10	0.86	0.04961	0.00255	0.25069	0.01369	0.03665	0.00087	177	114	227	11	232	5
	XB-1-2.17	125.81	207.43	0.61	0.05826	0.00286	0.30929	0.01631	0.03851	0.00092	539	97	274	13	244	6
	XB-1-2.18	70.87	123.40	0.57	0.04715	0.00313	0.24819	0.01734	0.03818	0.00103	57	131	225	14	242	6
	XB-1-2.19	140.76	225.37	0.62	0.04847	0.0026	0.25208	0.01426	0.03772	0.0009	122	114	228	12	239	6
	XB-1-2.20	105.00	196.16	0.54	0.04961	0.00293	0.25635	0.01584	0.03748	0.00094	177	130	232	13	237	6
	XB-1-2.21	83.89	139.40	0.60	0.05844	0.0038	0.30244	0.02024	0.03753	0.00106	546	124	268	16	238	7
	XB-1-2.22	98.99	153.53	0.64	0.0534	0.00312	0.283	0.01767	0.03844	0.00098	346	114	253	14	243	6
	XB-1-2.23	103.49	192.26	0.54	0.05814	0.00329	0.30176	0.01791	0.03764	0.00094	535	129	268	14	238	6
	XB-1-2.24	107.13	163.05	0.66	0.04983	0.00308	0.2637	0.01697	0.03838	0.00096	187	144	238	14	243	6
	XB-1-2.25	70.65	136.07	0.52	0.04638	0.00297	0.25051	0.01674	0.03917	0.00101	18	124	227	14	248	6
	XB-1-2.26	70.36	136.94	0.51	0.05486	0.00334	0.29142	0.0184	0.03853	0.00097	407	124	260	14	244	6
	XB-1-2.27	135.01	208.47	0.65	0.05043	0.0027	0.24777	0.01418	0.03563	0.00087	215	113	225	12	226	5
	XB-1-2.28	25.35	74.58	0.34	0.0615	0.00573	0.3227	0.02968	0.03806	0.00116	657	191	284	23	241	7
	XB-1-2.29	66.29	133.92	0.50	0.05537	0.00383	0.28903	0.02041	0.03786	0.00106	427	142	258	16	240	7
	XB-1-2.30	227.09	273.70	0.83	0.04991	0.00215	0.25875	0.01273	0.0376	0.00087	191	90	234	10	238	5
	XB-1-2.31	183.19	253.93	0.72	0.05436	0.00239	0.28433	0.01391	0.03793	0.0009	386	91	254	11	240	6
	XB-1-2.32	132.06	201.90	0.65	0.04991	0.00277	0.27074	0.01566	0.03934	0.00102	191	127	243	13	249	6
Wolihe Dingzi	WLH-1-10.01	140.01	259.25	0.54	0.05426	0.00248	0.27414	0.01239	0.03664	0.00081	382	99	246	10	232	5
	WLH-1-10.02	103.45	243.11	0.43	0.06361	0.00218	0.50059	0.02080	0.05708	0.00134	729	86	412	14	358	8
	WLH-1-10.03	36.87	127.98	0.29	0.0545	0.00394	0.28915	0.01973	0.03848	0.00098	392	162	258	16	243	6
	WLH-1-10.04	161.64	282.64	0.57	0.05055	0.00241	0.25823	0.01238	0.03705	0.00083	220	100	233	10	235	5
	WLH-1-10.05	82.23	168.30	0.49	0.05159	0.00351	0.25949	0.01706	0.03648	0.00094	267	142	234	14	231	6
	WLH-1-10.06	85.34	177.56	0.48	0.05224	0.00291	0.28128	0.01511	0.03905	0.00093	296	132	252	12	247	6
	WLH-1-10.07	287.32	390.07	0.74	0.05015	0.00223	0.2557	0.01128	0.03698	0.0008	202	105	231	9	234	5

listed in Table 2.

The SHRIMP zircon target preparation and CL image analysis and tests were undertaken using SHRIMP II ion probe at the Beijing SHRIMP Centre. The analytic method referred to the method established by existing researches (Williams, 1998). The TEMORA standard of Australian National University was taken as the internal standard, and the SL13 zircon standard (Sri Lankan gem zircon standard) (Black et al., 2003) was taken as the calculation standard. The common lead was corrected according to the method (Compston et al., 1992). The test results are listed in Table 3.

3.2.2 Petrological–geochemical test and results

The test and analysis of the major and trace elements were undertaken at the Analytical Laboratory, Beijing Research Institute of Uranium Geology. The major elements were analyzed using Philips PW2404 XRF. The FeO was measured using chemical capacity method. The trace elements were analyzed using Finnigan MAT Element I ICP-MS. The major and trace elements tested using GB/T 14506.28—93 silicate rock chemical analytic method and X-ray fluorescence spectrometry are the basis of the test. The test results are listed in Table 4.

4 Chronology and Geochemistry

4.1 Zircon U-Pb chronology

The zircons in the monzonitic granite (YJ–1–1) from the Yuejin rock body, monzonitic granite (XB–1–2) from

Table 2 (Contiued)

Location	No.	ω(B)/(ppm)		Th/U	Isotopic ratio						Age/(Ma)					
		Th	U		$^{207}Pb/^{206}Pb$	1σ	$^{207}Pb/^{235}U$	1σ	$^{206}Pb/^{238}U$	1σ	$^{207}Pb/^{206}Pb$	1σ	$^{207}Pb/^{235}U$	1σ	$^{206}Pb/^{238}U$	1σ
Wolihe Dingzi	WLH-1-10.08	67.06	173.10	0.39	0.04909	0.00257	0.26114	0.01372	0.03858	0.00092	152	118	236	11	244	6
	WLH-1-10.09	102.06	245.93	0.42	0.05145	0.00255	0.27654	0.01359	0.03899	0.00092	261	114	248	11	247	6
	WLH-1-10.10	110.89	238.47	0.46	0.05554	0.00303	0.29388	0.01598	0.03838	0.00091	434	121	262	13	243	6
	WLH-1-10.11	122.06	263.56	0.46	0.05337	0.00273	0.2876	0.01439	0.03909	0.0009	344	121	257	11	247	6
	WLH-1-10.12	158.66	271.13	0.59	0.05102	0.00249	0.27317	0.01295	0.03884	0.00087	242	117	245	10	246	5
	WLH-1-10.13	123.34	246.31	0.50	0.05235	0.00265	0.27298	0.01407	0.03782	0.0009	301	109	245	11	239	6
	WLH-1-10.14	76.15	202.51	0.38	0.06447	0.0035	0.33126	0.01845	0.03726	0.00088	757	110	291	14	236	5
	WLH-1-10.15	150.80	228.79	0.66	0.05887	0.00322	0.30849	0.01631	0.03801	0.00092	562	115	273	13	240	6
	WLH-1-10.16	121.82	235.48	0.52	0.05377	0.00266	0.27682	0.01354	0.03734	0.00087	361	107	248	11	236	5
	WLH-1-10.17	225.29	368.55	0.61	0.04979	0.00219	0.25662	0.01118	0.03738	0.00083	185	99	232	9	237	5
	WLH-1-10.18	57.31	186.54	0.31	0.05442	0.00305	0.28154	0.0156	0.03752	0.00092	388	123	252	12	237	6
	WLH-1-10.19	120.44	228.35	0.53	0.046	0.00243	0.23039	0.01192	0.03632	0.00085	-2	108	211	10	230	5
	WLH-1-10.20	100.13	227.84	0.44	0.05232	0.00275	0.27099	0.01403	0.03757	0.00088	299	115	243	11	238	5
	WLH-1-10.21	106.42	204.77	0.52	0.05129	0.00263	0.26647	0.01335	0.03768	0.00088	254	113	240	11	238	5
	WLH-1-10.22	82.47	198.60	0.42	0.04835	0.00266	0.25374	0.01333	0.03806	0.00091	116	124	230	11	241	6
	WLH-1-10.23	159.42	282.94	0.56	0.05376	0.00246	0.27907	0.01264	0.03765	0.00085	361	106	250	10	238	5
	WLH-1-10.24	128.91	252.54	0.51	0.05871	0.00200	0.62714	0.02570	0.07748	0.00177	556	84	494	16	481	11
	WLH-1-10.25	114.28	254.21	0.45	0.0494	0.00237	0.2516	0.01213	0.03694	0.00087	167	105	228	10	234	5
	WLH-1-10.26	72.77	191.93	0.38	0.04719	0.00262	0.24484	0.01353	0.03763	0.00089	59	109	222	11	238	6
	WLH-1-10.27	178.45	271.56	0.66	0.05212	0.00245	0.27789	0.01312	0.03867	0.0009	291	99	249	10	245	6
	WLH-1-10.28	118.15	228.82	0.52	0.0538	0.00258	0.28475	0.01353	0.03839	0.00087	363	102	254	11	243	5
	WLH-1-10.29	106.02	193.00	0.55	0.05372	0.00264	0.27651	0.01351	0.03733	0.00089	359	105	248	11	236	6
	WLH-1-10.30	91.50	210.72	0.43	0.05117	0.0026	0.2705	0.01372	0.03834	0.00089	249	108	243	11	243	6
	WLH-1-10.31	66.55	169.66	0.39	0.05144	0.00289	0.2613	0.01444	0.03684	0.00087	261	120	236	12	233	5
	WLH-1-10.32	167.37	226.55	0.74	0.05706	0.00289	0.28923	0.01478	0.03676	0.0009	494	105	258	12	233	6
Xiao Duobaoshan	XDB-1-1.01	391.83	319.51	1.23	0.06164	0.00759	0.2821	0.03524	0.03319	0.00083	662	258	252	28	211	5
	XDB-1-1.02	52.85	103.96	0.51	0.0504	0.00663	0.26082	0.03467	0.03753	0.00105	214	266	235	28	238	7
	XDB-1-1.03	117.61	201.59	0.58	0.0549	0.00693	0.27057	0.03465	0.03574	0.00093	408	271	243	28	226	6
	XDB-1-1.04	76.91	136.38	0.56	0.05901	0.0076	0.29012	0.03772	0.03566	0.00097	567	274	259	30	226	6
	XDB-1-1.05	106.87	178.24	0.60	0.05746	0.00721	0.2738	0.03486	0.03456	0.00091	509	283	246	28	219	6
	XDB-1-1.6	330.85	247.64	1.34	0.05293	0.00659	0.25894	0.03272	0.03548	0.0009	326	266	234	26	225	6
	XDB-1-1.7	75.98	187.53	0.41	0.06142	0.00746	0.63376	0.07832	0.07484	0.00185	654	282	498	49	465	11
	XDB-1-1.8	104.62	156.01	0.67	0.06709	0.00874	0.32133	0.04209	0.03474	0.00098	841	298	283	32	220	6
	XDB-1-1.9	116.89	161.98	0.72	0.05755	0.00727	0.2749	0.03542	0.03465	0.00095	513	285	247	28	220	6
	XDB-1-1.10	177.22	213.00	0.83	0.06906	0.0085	0.33569	0.04187	0.03525	0.00089	901	278	294	32	223	6

Table 3 Statistic results of the SHRIMP zircon U-Pb ages of the Tongshan rock body

Sample No.	w(B)/(ppm)		Th/U	Isotopic ratio						Age/(Ma)					
	Th	U		$^{207}Pb/^{206}Pb$	1σ	$^{207}Pb/^{235}U$	1σ	$^{206}Pb/^{238}U$	1σ	$^{207}Pb/^{206}Pb$	1σ	$^{207}Pb/^{235}U$	1σ	$^{206}Pb/^{238}U$	1σ
TS02-3-5	96.70	167.34	0.60	0.0483	0.00773	0.234	0.03744	0.03520	0.00060	113	370	223	23	223.0	3.7
TS02-3-6	82.32	210.53	0.40	0.0479	0.00398	0.231	0.01940	0.03496	0.00052	96	200	197	17	221.5	3.3
TS02-3-13	79.86	152.57	0.54	0.042	0.00151	0.199	0.00716	0.03446	0.00079	-237	910	173	50	218.4	5.0
TS02-3-14	57.93	121.59	0.49	0.0612	0.00796	0.308	0.04312	0.03647	0.00066	646	290	263	30	230.9	4.1
TS02-3-15	51.75	96.69	0.55	0.034	0.00184	0.161	0.00869	0.03412	0.00096	-770	1500	148	62	216.3	6.0
TS02-3-16	76.77	155.13	0.51	0.050	0.00175	0.237	0.00830	0.03464	0.00087	178	820	186	64	219.5	5.4
TS02-3-17	76.08	156.79	0.50	0.046	0.00106	0.224	0.00515	0.03539	0.00064	-3	560	217	37	224.2	4.1
TS02-3-18	92.56	167.64	0.57	0.0579	0.00423	0.283	0.02094	0.03546	0.00053	526	160	234	14	224.7	3.3

the 173-kilometer rock body, and monzonitic granite (WLH–1–10) from the Wolihedingzi rock body occur as long columns of (40 μm×60 μm)−(45 μm×160 μm) in size, with a length/width ratio of 1.16−3.56. The zircons are subhedral–euhedral, with perfect crystal form and relatively clean surface, and exhibits obvious magmatic oscillatory zoning (Fig. 3). The contents of ^{232}Th vary from 25.35 ppm to 287.32 ppm; the contents of ^{238}U vary from 36.87 ppm to 314.79 ppm; and the Th/U ratios are between 0.29 and 0.87, much larger than 0.1 (Table 2), belonging to typical magmatic zircon. In the test of YJ–1–1, if the test points No. 4, 15 and 21 with relatively high age errors are excluded, the age error ellipes of the 29 points show a relatively tight cluster on the concordia plots, the ^{206}Pb/^{238}U ages range from 227±5 Ma to 252±6 Ma, and the weighted mean age is 238.1±2.4 Ma (MSDW=1.16) (Figs. 4a and 4b; Table 2). In the test of XB–1–2, if the test points No. 1, 7 and 10 with relatively high age errors are excluded, the age error ellipes of the 29 points show a relatively tight cluster on the concordia plots; the ^{206}Pb/^{238}U ages range from 226±5 Ma to 249±6 Ma, and the weighted mean age is 238.5±2.1 Ma

Table 4 Test results of the major elements (wt%) and trace elements (ppm) in the rock bodies

No.	Yuejin			173-kilometer			Wolihedingzi			Tongshan			Xiaoduobaoshan		
	YJ-1-2	YJ-1-3	YJ-1-7	XB-1-5	XB-1-6	XB-1-7	WLH-1-13	WLH-1-14	WLH-1-16	TS-02-2	TS-02-5	TS-02-6	XDB-1-5	XDB-1-6	XDB-1-7
SiO_2	70.52	73.58	69.72	72.39	73.61	74.58	71.19	73.28	72.78	67.8	67.17	68.26	68.14	67.73	68.05
TiO_2	0.22	0.24	0.2	0.27	0.22	0.21	0.3	0.06	0.27	0.55	0.42	0.41	0.58	0.59	0.58
Al_2O_3	15.47	13.91	15.36	16.45	14.6	14.78	15.65	14.73	14.54	14.9	15.38	15.24	14.73	13.91	14.14
Fe_2O_3	2.64	1.52	3.63	1.12	0.99	1.08	1.88	1.5	1.91	1.77	1.84	2.2	2.04	2.2	2.07
FeO	0.27	0.22	0.26	0.24	0.35	0.17	0.26	0.14	0.18	1.24	1.22	0.57	1.78	1.62	1.66
MnO	0.02	0.04	0.03	0.02	0.03	0.03	0.01	0.02	0.04	0.08	0.04	0.05	0.07	0.07	0.06
MgO	0.32	0.26	0.37	0.62	0.58	0.36	0.26	0.02	0.24	1.6	1.64	1.49	2.12	3.18	3.01
CaO	0.23	0.62	0.19	0.19	0.91	0.28	0.25	0.46	0.45	2.3	2.17	1.9	2.43	2.84	2.5
Na_2O	5.75	5.36	5.47	3.4	5.29	4.69	4.57	4.55	5.11	4.39	4.65	4.76	4.58	4.3	4.19
K_2O	2.8	2.69	2.88	3.04	2.04	2.02	3.42	3.76	2.68	2.88	2.94	2.89	1.93	1.68	1.96
P_2O_5	0.077	0.067	0.08	0.057	0.064	0.074	0.084	0.018	0.094	0.206	0.159	0.177	0.155	0.152	0.156
LOI	1.56	1.16	1.66	2.1	1.24	1.64	1.92	1.18	1.48	2.16	2.24	2.1	1.62	1.54	1.5
Total	99.88	99.67	99.85	99.89	99.92	99.92	99.8	99.72	99.77	99.88	99.86	100.04	100.17	99.81	99.88
Na_2O+K_2O	8.55	8.05	8.35	6.44	7.33	6.71	7.99	8.31	7.79	7.27	7.59	7.65	6.51	5.98	6.15
A/CNK	1.20	1.08	1.23	1.78	1.16	1.42	1.34	1.19	1.20	1.02	1.04	1.06	1.05	0.99	1.04
A/NK	1.24	1.19	1.27	1.85	1.34	1.49	1.39	1.27	1.29	1.44	1.42	1.39	1.53	1.56	1.57
R1	1953	2352	1959	2925	2539	2840	2305	2377	2386	2241	2093	2142	2379	2518	2513
R2	350	357	346	382	418	344	354	344	351	632	630	588	664	747	706
La	18.55	12.10	9.97	20.90	12.60	15.10	5.22	8.82	25.90	21.57	21.30	15.90	16.40	16.60	17.00
Ce	37.00	29.80	21.70	35.40	31.70	28.30	8.66	13.70	34.50	45.40	40.70	32.70	33.80	34.15	34.60
Pr	5.42	2.78	2.81	4.54	3.03	3.60	0.94	2.10	4.02	5.78	5.26	4.12	4.45	4.41	4.53
Nd	20.15	10.40	10.80	15.80	11.10	13.50	3.09	7.64	11.70	22.73	19.90	15.95	17.30	17.65	18.00
Sm	3.08	1.68	1.90	2.05	1.67	2.15	0.47	1.22	1.40	4.05	3.41	2.90	3.40	3.28	3.40
Eu	0.45	0.43	0.36	0.56	0.47	0.62	0.11	0.30	0.28	1.18	1.01	0.86	0.98	0.95	0.94
Gd	1.97	1.13	1.46	1.40	1.19	1.41	0.32	0.84	1.13	3.26	2.50	2.27	2.84	2.76	2.76
Tb	0.27	0.16	0.21	0.19	0.16	0.20	0.06	0.14	0.17	0.47	0.36	0.32	0.42	0.40	0.39
Dy	1.14	0.74	1.09	0.83	0.74	0.86	0.30	0.67	0.80	2.38	1.71	1.58	2.04	1.99	1.95
Ho	0.21	0.15	0.22	0.16	0.13	0.17	0.07	0.14	0.16	0.48	0.32	0.32	0.43	0.39	0.38
Er	0.67	0.43	0.71	0.50	0.40	0.53	0.28	0.47	0.56	1.44	1.04	1.00	1.20	1.20	1.14
Tm	0.09	0.06	0.10	0.07	0.05	0.07	0.05	0.06	0.08	0.19	0.13	0.13	0.16	0.16	0.15
Yb	0.61	0.38	0.73	0.43	0.37	0.46	0.38	0.53	0.60	1.29	0.95	0.93	1.09	1.06	1.01
Lu	0.10	0.06	0.12	0.07	0.06	0.07	0.09	0.10	0.11	0.20	0.15	0.14	0.17	0.17	0.16
Y	6.12	3.96	6.48	4.86	3.82	4.56	2.43	4.03	5.29	13.60	9.86	8.86	11.70	11.10	10.80
ΣREE	89.68	60.30	52.18	82.90	63.67	67.04	85.99	81.41	78.60	110.42	98.74	79.09	84.68	85.13	86.41
LREE	84.64	57.19	47.54	79.25	60.57	63.27	81.20	77.80	71.95	100.71	91.58	72.42	76.33	77.03	78.47
HREE	5.04	3.11	4.64	3.65	3.10	3.77	4.79	3.61	6.65	9.71	7.16	6.67	8.35	8.10	7.94
LREE/HREE	16.79	18.39	10.25	21.71	19.54	16.78	16.95	21.55	10.82	10.38	12.79	10.86	9.14	9.51	9.88
La_N/Yb_N	21.81	22.84	9.80	34.86	24.43	23.55	20.85	29.17	11.55	12.02	16.08	12.26	10.79	11.29	12.07
La_N/Sm_N	3.89	4.65	3.39	6.58	4.87	4.53	3.80	10.74	2.88	3.43	4.03	3.55	3.11	3.27	3.23
Gd_N/Lu_N	2.43	2.33	1.50	2.47	2.45	2.49	2.53	1.53	2.21	2.01	2.06	2.00	2.06	2.07	2.13
δEu	0.52	0.90	0.64	0.96	0.97	1.02	0.92	0.65	0.85	0.96	1.01	0.99	0.94	0.94	0.91
δCe	0.89	1.21	0.99	0.85	1.22	0.91	0.92	0.78	0.92	0.98	0.92	0.97	0.95	0.96	0.95
Rb	30.85	34.70	37.40	41.50	23.50	26.20	37.65	69.9	26.2	56.70	46.20	46.35	30.70	28.85	33.40
Ba	212.00	428.00	229.00	197.00	688.00	308.00	77.7	36	239	596.00	382.00	387.50	717.00	580.00	666.00
Th	3.50	1.81	1.85	2.18	2.10	1.86	2	10.4	1.43	4.23	4.41	4.18	3.38	3.47	3.61
U	0.64	0.55	0.77	1.69	0.65	0.83	1.27	1.41	0.75	1.13	1.39	1.47	1.25	1.45	1.37
Nb	3.95	3.53	3.26	3.60	3.06	3.03	3.88	3.2	3.37	4.42	3.78	3.52	4.07	4.18	4.26
Ta	0.20	0.21	0.20	0.22	0.19	0.17	0.19	0.11	0.19	0.26	0.30	0.23	0.27	0.25	0.26
K	23244	22330	23908	25236	16935	16769	28391	31214	22248	23908	24406	23991	16022	13946	16271
Pb	5.89	9.46	5.95	20.80	13.60	18.30	10.66	23.8	11.3	23.40	26.30	19.45	14.30	29.45	21.20
Sr	176.50	476.00	166.00	353.00	792.00	742.00	126.5	35.9	386	470.00	269.00	214.00	919.00	933.00	867.00
P	336	294	347	250	277	325	367	79	410	898	696	774	676	662	679
Zr	257.00	224.00	353.00	248.00	214.00	255.00	266	122	238	339.33	328.00	294.50	401.00	347.50	325.00
Hf	7.76	6.46	10.60	7.26	6.08	8.22	8.02	4.15	7.61	10.19	10.10	9.08	12.00	10.63	9.93
Ti	1331	1466	1226	1590	1305	1282	1797	359	1618	3276	2501	2432	3468	3530	3494

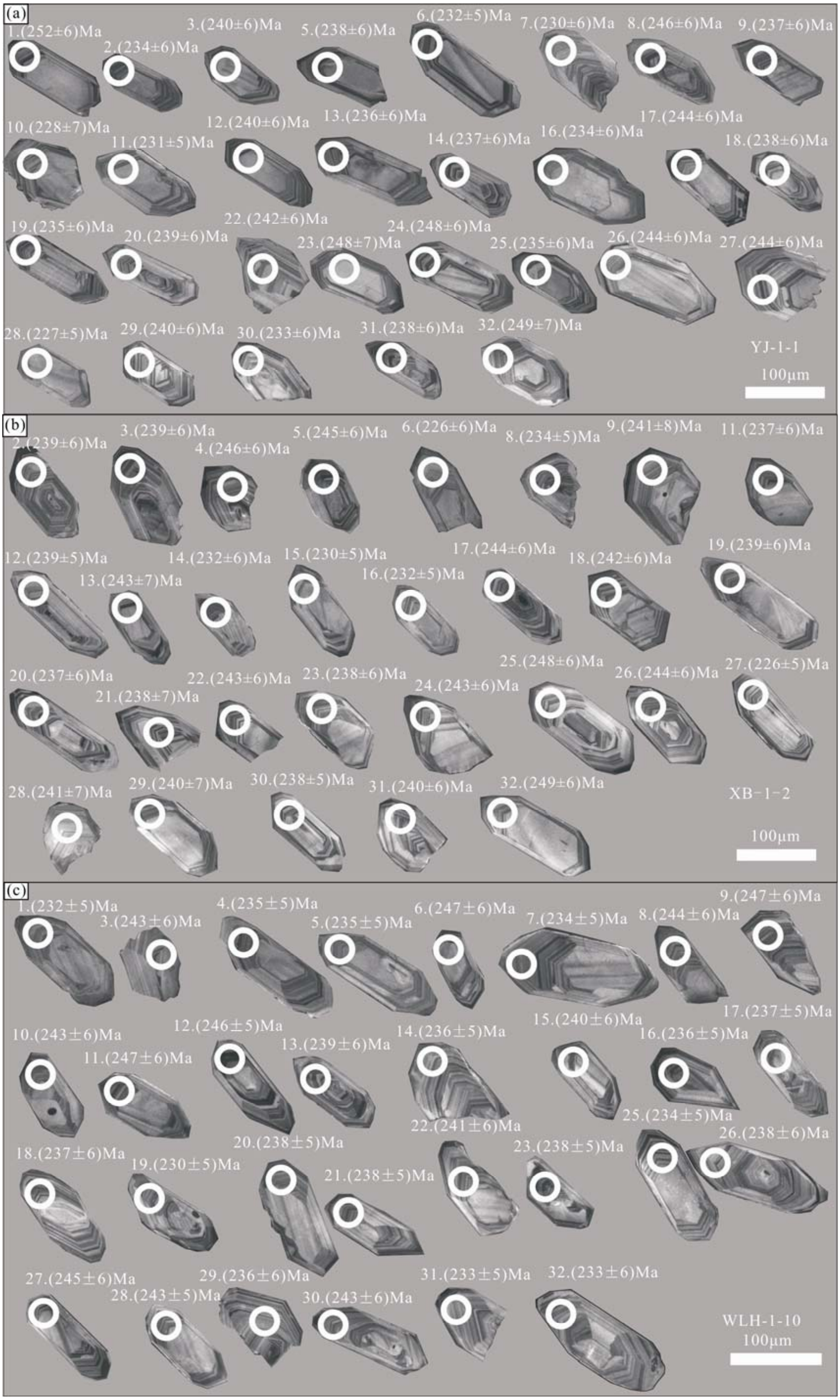
(a)
1.(252±6)Ma
2.(234±6)Ma
3.(240±6)Ma
5.(238±6)Ma
6.(232±5)Ma
7.(230±6)Ma
8.(246±6)Ma
9.(237±6)Ma
10.(228±7)Ma
11.(231±5)Ma
12.(240±6)Ma
13.(236±6)Ma
14.(237±6)Ma
16.(234±6)Ma
17.(244±6)Ma
18.(238±6)Ma
19.(235±6)Ma
20.(239±6)Ma
22.(242±6)Ma
23.(248±7)Ma
24.(248±6)Ma
25.(235±6)Ma
26.(244±6)Ma
27.(244±6)Ma
28.(227±5)Ma
29.(240±6)Ma
30.(233±6)Ma
31.(238±6)Ma
32.(249±7)Ma
YJ-1-1
100μm
(b)
2.(239±6)Ma
3.(239±6)Ma
4.(246±6)Ma
5.(245±6)Ma
6.(226±6)Ma
8.(234±5)Ma
9.(241±8)Ma
11.(237±6)Ma
12.(239±5)Ma
13.(243±7)Ma
14.(232±6)Ma
15.(230±5)Ma
16.(232±5)Ma
17.(244±6)Ma
18.(242±6)Ma
19.(239±6)Ma
20.(237±6)Ma
21.(238±7)Ma
22.(243±6)Ma
23.(238±6)Ma
24.(243±6)Ma
25.(248±6)Ma
26.(244±6)Ma
27.(226±5)Ma
28.(241±7)Ma
29.(240±7)Ma
30.(238±5)Ma
31.(240±6)Ma
32.(249±6)Ma
XB-1-2
100μm
(c)
1.(232±5)Ma
3.(243±6)Ma
4.(235±5)Ma
5.(235±5)Ma
6.(247±6)Ma
7.(234±5)Ma
8.(244±6)Ma
9.(247±6)Ma
10.(243±6)Ma
11.(247±6)Ma
12.(246±5)Ma
13.(239±6)Ma
14.(236±5)Ma
15.(240±6)Ma
16.(236±5)Ma
17.(237±5)Ma
18.(237±6)Ma
19.(230±5)Ma
20.(238±5)Ma
21.(238±5)Ma
22.(241±6)Ma
23.(238±5)Ma
25.(234±5)Ma
26.(238±6)Ma
27.(245±6)Ma
28.(243±5)Ma
29.(236±6)Ma
30.(243±6)Ma
31.(233±5)Ma
32.(233±6)Ma
WLH-1-10
100μm

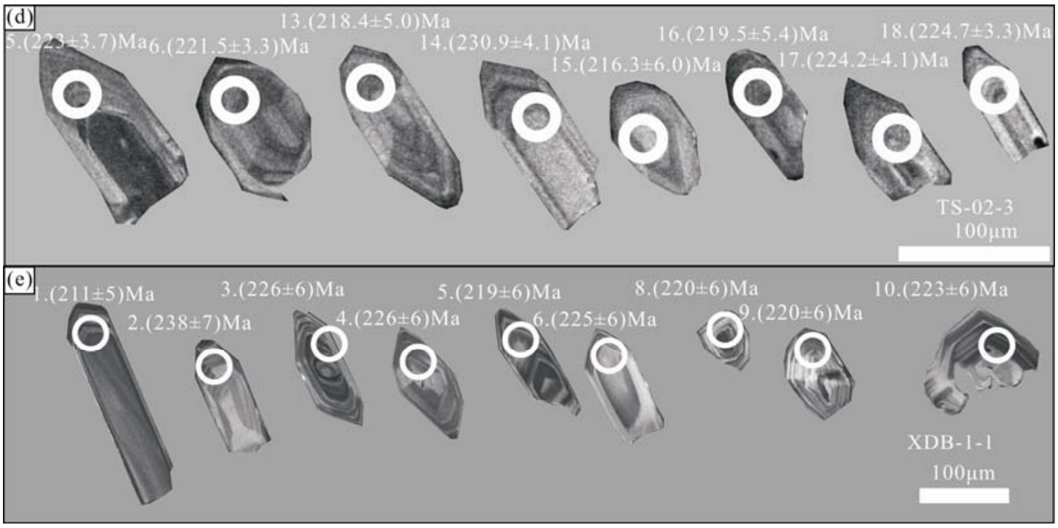

Fig. 3. CL images of the zircons.
(a), Monzonitic granite from the Yuejing rock body (YJ-1-1); (b), Monzonitic granite from the 173-kilometer rock body (XB-1-2); (c), Monzonitic granite from the Wolihedingzi rock body (WLH-1-10); (d), Granodiorite from the Tongshan rock body (TS-02-3); (e), Granodiorite porphyry from the Xiaoduobaoshan rock body (XDB-1-1).

(MSDW=1.05) (Figs. 4c and 4d; Table 2). In the test of WLH–1–10, if the test points No. 2 and 24 with relatively high errors are excluded, the age error ellipes of the 30 points show a relatively tight cluster on the concordia plot; the ^{206}Pb/^{238}U ages range from 232±5 Ma to 247±6 Ma, and the weighted mean age is 238.4±2.0 Ma (MSDW=0.72) (Figs. 4e and 4f; Table 2). The diagenetic age of the tonolite belongs to Indosinian.

The zircon in the granodiorite (TS–02–3) from the Tongshan rock body occurs dominantly as short columns and minor long columns, with sizes between 30 μm×40 μm and 40 μm×200 μm and a length/width ratio varying from 1.33 to 5.00. The zircon is euhedral, with a clean surface, and exhibits obvious magmatic oscillatory zoning (Fig. 3d). The contents of ^{232}Th range from 51.75 ppm to 391.83 ppm; the contents of ^{238}U vary from 96.68 ppm to 319.51 ppm; and the Th/U ratios are between 0.40 and 1.34, much larger than 0.1 (Table 3), belonging to typical magmatic zircon. The age error ellipes of the eight points show a relatively tight cluster on the concordia plots. The ^{206}Pb/^{238}U ages range from 216.3 Ma to 230.9 Ma, and the weighted mean age is 223.1±2.8 Ma (n=8, MSWD=0.96) (Figs. 4g and 4h; Table 3), indicating that the diagenetic age of the granodiorite belongs to Indosinian. In the test of XDB–1–1, if the seven test points with relatively high age errors are excluded, the age error ellipes of the nine points show a relatively tight cluster on the concordia plots; the ^{206}Pb/^{238}U ages range from 211±5 Ma to 238±7 Ma, and the weighted mean age is 222.1±5.5 Ma (n=9, MSWD=1.5) (Figs. 4i and 4j; Table 2), indicating that the diagenetic age of the granodiorite belongs to Indosinian.

4.2 Petrological-geochemical characteristics

According to Fig. 5, Fig. 6 and Table 4, the SiO_2 contents in the monzonitic granite (No. YJ–1–2, YJ–1–3 and YJ–1–7) from the Yuejin rock body, the monzonitic granite (No. XB–1–5, XB–1–6 and XB–1–7) from the 173 -kilometer rock body and the monzonitic granite (No. WLH–1–8, WLH–1–9 and WLH–1–14) from the Wolihedingzi rock body vary from 69.72wt% to 74.58wt%, falling into granite field in the TAS diagram. The K_2O contents are slightly high, ranging from 2.02wt% to 3.76wt%; they are especially high in samples from Wolihedingzi rock body (3.4wt% to 5.75wt%). The total alkali contents of Na_2O+K_2O are between 6.44wt% and 8.55wt%, which mainly belong to calc–alkaline series while samples from Wolihedingzi rock body belong to transition zone of high-K cal–alkaline series and cal–alkaline series. The Al_2O_3 contents are relatively high, ranging from 13.91wt% to 15.47wt%, and the aluminum saturation index A/CNK of the rocks is between 1.08 and 1.78, belonging to peraluminous rock in the A/CNK–A/NK diagram. The total rare earth contents ΣREE range from 52.18 ppm to 89.68 ppm, while those of the LREE vary from 47.54 ppm to 84.64 ppm, and those of HREE vary from 3.11 ppm to 6.65 ppm. The LREE/HREE ratios are between 10.25 and 21.71; the La_N/Yb_N ratios range from 9.80 to 34.86; the La_N/Sm_N ratios range from 1.50 to 6.58, and the δEu values range from 0.52 to 1.02; δCe values range from 0.78 to 1.22, which exhibit the features of right–inclined type, LREE enrichment, steeply dipping curve and relatively stable HREE content as well as presence of obvious negative Eu anormaly in the rare earth distribution diagram. In the spider diagram of the trace elements, Pb, Zr and Hf in samples from YJ–1–2, YJ–1–3 and YJ–1–7 are relatively enriched, while Nb and Ta are relatively depleted. Ba, U, Pb, Sr, Zr and Hf in the samples from XB–1–5, XB–1–6 and XB–1–7 are relatively enriched, while Nb, Ta and Ti are relatively depleted. Pb, Zr and Hf in the samples from WLH–1–8, WLH–1–9 and WLH–1–14 are relatively enriched, while Ba, Nb, Ta and Ti are relatively depleted.

The SiO_2 contents in the granodiorite (No. Ts02–2, Ts02–5 and Ts02–6) from the Tongshan rock body and the granodiorite porphyry (No. XDB–1–5, XDB–1–6 and XDB–1–7) from the Xiaoduobaoshan rock body range from 64.77wt% to 68.26wt%, falling near the boundary line between granodiorite and quartz monzonite in the

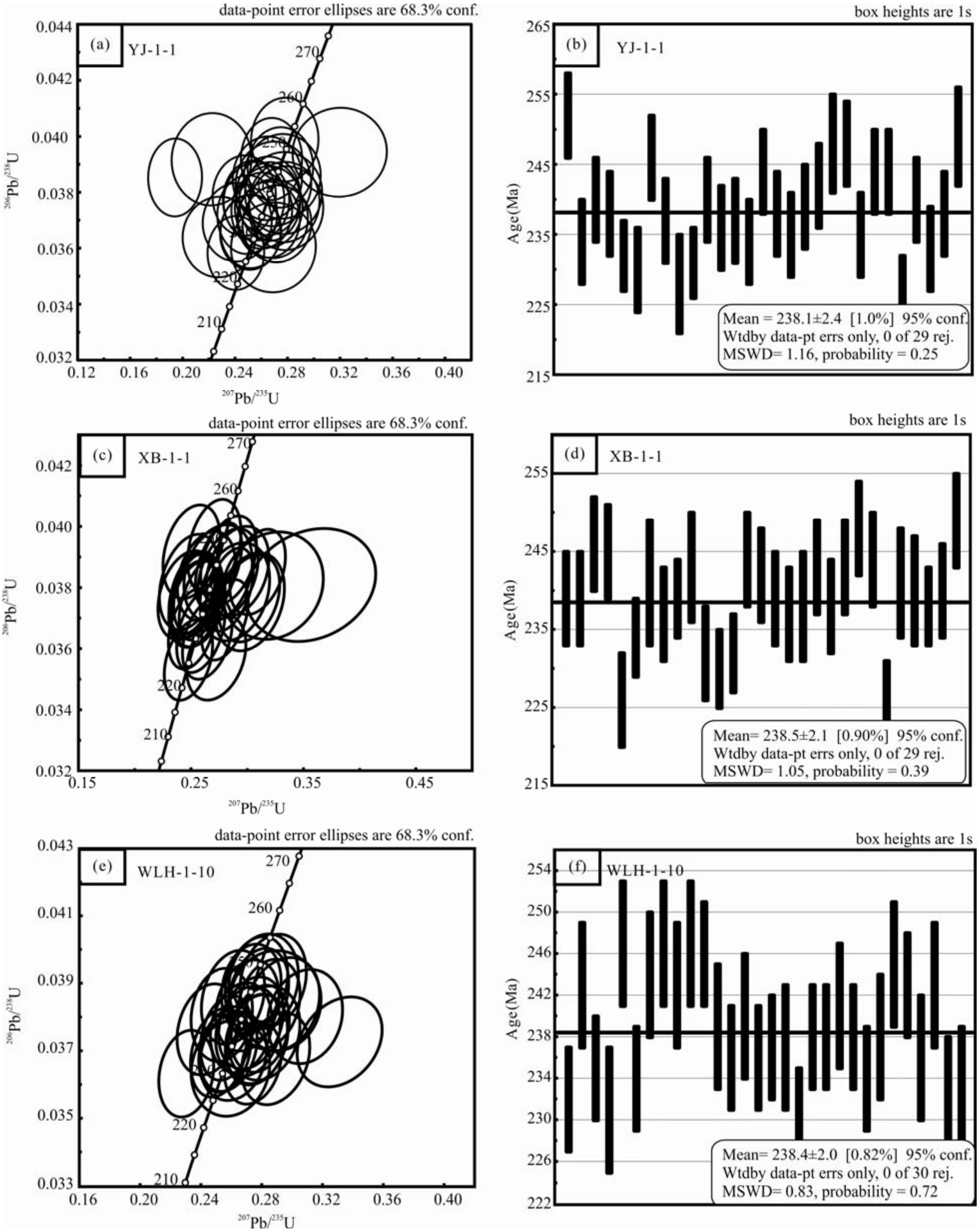

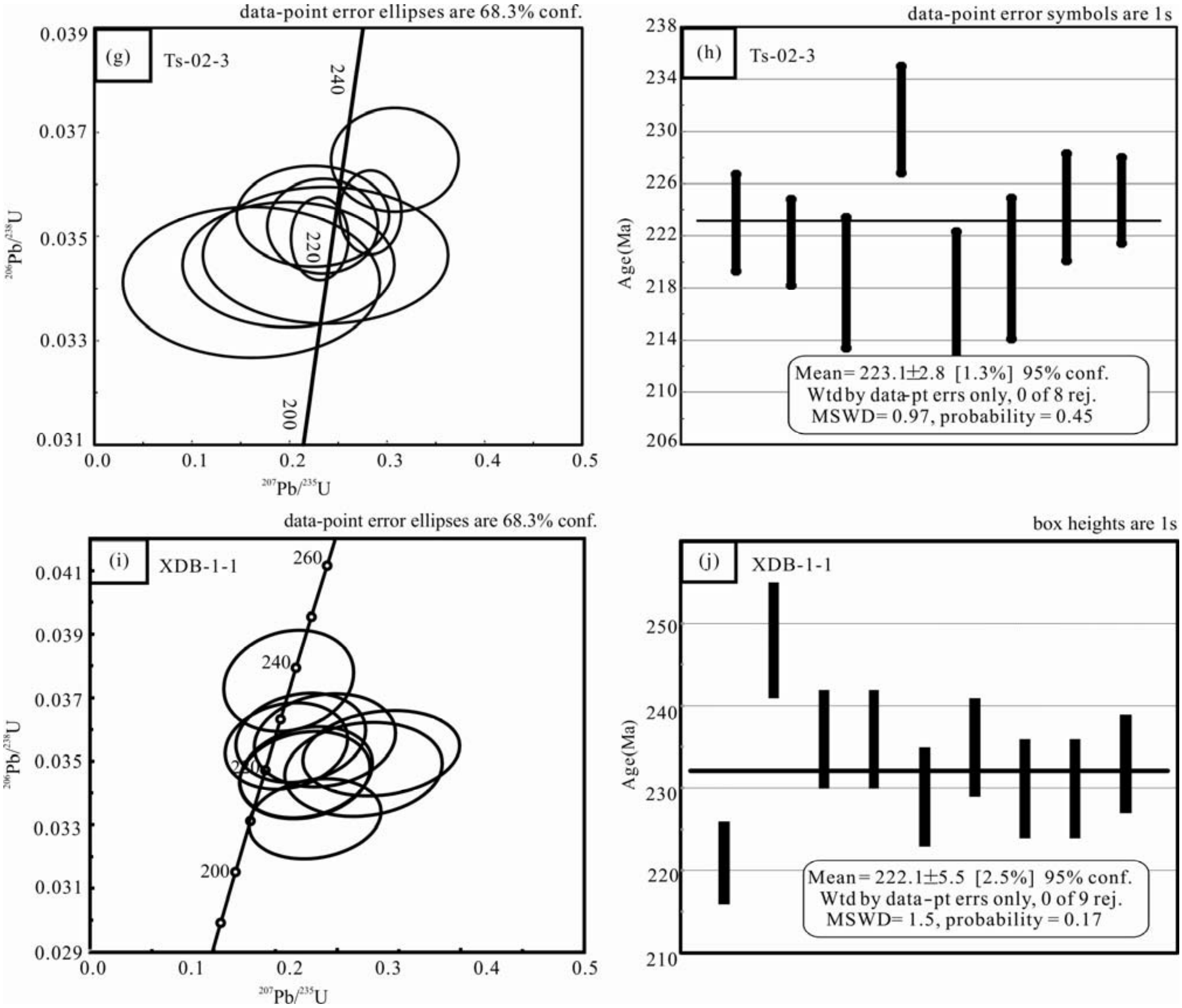

Fig. 4. Zircon U-Pb concordia diagrams and $^{206}Pb/^{238}U$ age spectra.
(a), Monzonitic granite zircon U-Pb concordia diagram from the Yuejing rock body (YJ-1-1); (b), Monzonitic granite $^{206}Pb/^{238}U$ age spectrum from the Yuejing rock body (YJ-1-1); (c), Monzonitic granite zircon U-Pb concordia diagram from the 173-kilometer rock body (XB-1-2); (d), Monzonitic granite $^{206}Pb/^{238}U$ age spectrum from the 173-kilometer rock body (XB-1-2); (e), Monzonitic granite zircon U-Pb concordia diagram from the Wolihedingzi rock body (WLH-1-10); (f), Monzonitic granite $^{206}Pb/^{238}U$ age spectrum from the Wolihedingzi rock body (WLH-1-10); (g), Granodiorite zircon U-Pb concordia diagram from the Tongshan rock body (TS-02-3); (h), Granodiorite $^{206}Pb/^{238}U$ age spectrum from the Tongshan rock body (TS-02-3); (i), Granodiorite porphyry zircon U-Pb concordia diagram from the Xiaoduobaoshan rock body (XDB-1-1); (j), Granodiorite porphyry $^{206}Pb/^{238}U$ age spectrum from the Xiaoduobaoshan rock body (XDB-1-1).

TAS diagram. The K_2O contents are relatively low, ranging from 1.68wt% to 3.02wt%, and the total alkali contents of Na_2O+K_2O vary from 5.98wt% to 7.65wt%, belonging to high-K calc–alkaline series in the SiO_2–K_2O diagram. The CaO contents are relatively high, ranging from 1.9wt% to 2.84wt%. The MgO contents are relatively high, ranging from 1.49wt% to 3.18wt%. The Al_2O_3 contents are high, ranging from 13.91wt% to 16.24wt%, and the aluminum saturation index A/CNK values are between 0.99 and 1.06, falling into the field of peraluminous rock in the A/CNK–A/NK diagram. The total rare earth contents ΣREE range from 79.09 ppm to 110.42 ppm. The LREE contents vary from 65.84 ppm to 91.58 ppm, and the HREE contents vary from 6.67 ppm to 8.35 ppm. The LREE/HREE ratios range from 9.14 to 12.79; the La_N/Yb_N ratios range from 10.79 to 16.08; the La_N/Sm_N ratios range from 3.11 to 4.03; the δEu values are 0.91−1.01, and the δCe values are 0.92−0.98, which exhibit the features of right–inclined type, LREE enrichment, steeply dipping curve and relatively stable HREE content in the rare earth distribution diagram. In the spider diagram of the trace elements, Pb, Zr and Hf in the samples from Ts02–2, Ts02–5 and Ts02–6 are relatively enriched, while Nb Ta and Ti are relatively depleted. Ba, U, Pb, Zr and Hf in the samples XDB–1–5, XDB–1–6 and XDB–1–7 are relatively enriched, while Nb Ta and Ti are relatively depleted.

5 Discussions

5.1 Determination of Indosinian

We carried out chronological study in five rock bodies. It is previously suggested that these rock bodies were formed in Variscan, but we believe that they were formed in Indosinian. The difference in the formation ages may be caused by the fact that previous workers made whole-rock dating using K-Ar method and yielded the mixed age of the rock bodies which is not accurate enough. The previous worker insisted in that the Yuejin and Xiaoduobaoshan rock bodies and related Cu-Mo deposits (occurrences) were formed in Variscan (Zhao Yiming et al., 1997). However, the new ages yielded by this study by high-precision zircon dating on the two deposits (occurrences) range from 238.1±2.4 Ma to 222.1±5.5 Ma (Table 2; Figs. 4a, 4b, 4i and 4j), not belonging to Variscan but Indosinian. In addition, in this study the age yielded by dating the sample collected in the granodiorite in the Tongshan ore district is 223.1±2.8 Ma (Table 3; Figs. 4g and 4h), also belonging to Indosinian; and the ages yielded by dating the samples from the 173-kilometer and Wolihedingzi rock bodies range from 238.5±2.1 Ma to 238.4±2.0 Ma (Table 2; Figs. 4c, 4d, 4e and 4f), which are consistent with those of the Yuejin rock body. All these indicate the Indosinian magmatic activities in the deposit cluster, and that the magmatic activities have important metallogenic significance.

Furthermore, the Indosinian diagenetic and metallogenic events in the whole Great Xing'an Range region are not isolated. The molybdenite Re-Os isochron age yielded in an associated Mo orebody in the Jinchanggouliang Au deposit (at the northern margin of the North China craton), Inner Mongolia in recent years is 244.7±2.5 Ma (Jiang Sihong et al., in print). Both the zircon age determined in the rock body and the

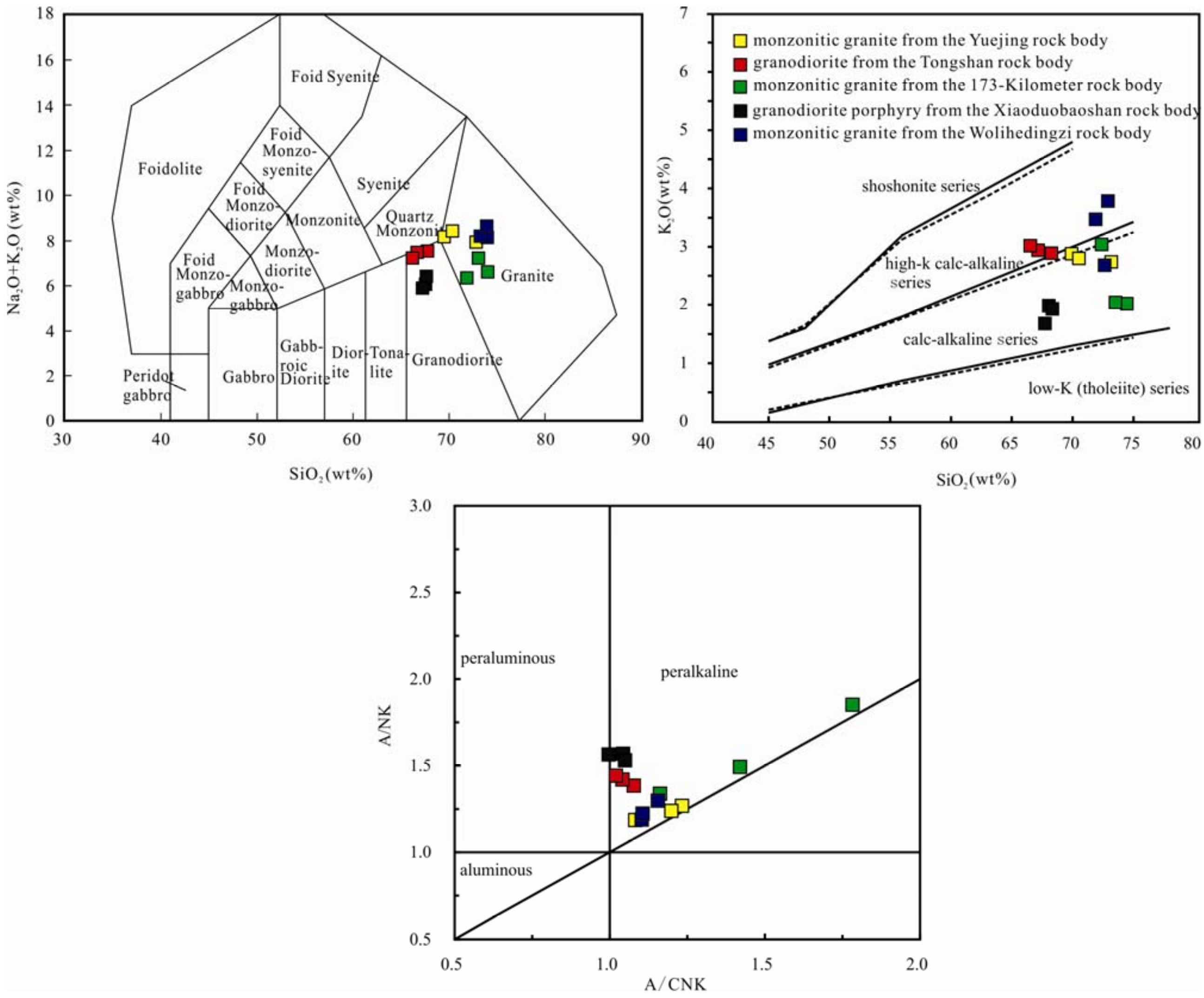

Fig. 5. SiO_2-K_2O diagram (Middlemost, 1994), TAS rock classification diagram (Peccerillo et al., 1976) and A/CNK-A/NK diagram (Manial et al., 1989).

molybdenite Re-Os age determined in the ore from the Chehugou porphyry Mo deposit (in the Xilamulun metallogenic belt at the north margin of the North China craton), Inner Mongolia are 245 Ma, and the zircon age of granite porphyry yielded by SHRIMP dating is 245±2.7 Ma (Zhang Lianchang et al., 2009). The zircon U-Pb age determined in the granodiorite from the Jiguanshan porphyry Al deposit (in the Xilamulun metallogenic belt at the north margin of the North China craton), Inner Mongolia is 245±2.7 Ma (Zeng Chingdong et al., 2009). The zircon U-Pb age determined in the granodiorite from the Baiyinnuoer Pb-Zn deposit (in the central segment of the Great Xing'an Range) , Inner Mongolia is 244.5±0.9 Ma (Jiang Sihong et al., 2011). The ages determined in the intrusive rocks in the Badaguan ore district (in the Erguna block at the south margin of the Mongolia–Okhotsk orogen), Inner Mongolia range from 243.87 Ma to 229 Ma (Kang Yongjian et al., 2014). The zircon U-Pb ages determined in an acid–intermediate intrusive bodies in Genhe, Mordaga and Jiuca areas (in the central segment of the Great Xing'an Range) concentrate between 241 Ma and 247 Ma (Tang et al., 2014). The zircon U-Pb ages of the gneissic granite in the northern part of Mordaga, monzogranite in Tayuan, syengranite in the west part of Mengui, quartz–feldspar veins in Guanhu Zhan and quartz diorite in Kutiankan (in the north segment of the Great Xing'an Range) are 243.9±4.2 Ma, 220±3 Ma, 220±3 Ma, 249±4 Ma and 244±4 Ma, respectively (She Hongquan et al., 2012).

Therefore, the fact that Indosinian magmatic activities occurred and formed deposits in the Duobaoshan ore concentration area provides further evidence for the Indosinian magmatic activities in the Great Xing'an Range region(Yang Huaben et al., 2016). The discovery of the Indosinian magmatic activities and metallogesis in the Duobaoshan ore concentration area can improve understanding of the magmatic evolution in the whole deposit cluster, and help to further study the metallogenic complexity and further supplement the metallogenic regularity in the deposit cluster.

5.2 Structural evolution and geological dynamic setting

The test data of the monzonitic granite samples (No. YJ–1–2, YJ–1–3 and YJ–1–7) from the Yuejin rock body, granodiorite samples (No. Ts02–2, Ts02–5 and Ts02–6) from the Tongshan rock body, monzonitic granite samples (No. XB–1–5, XB–1–6 and XB–1–7) from the 173-kilometer rock body, granodiorite porphyry samples (No. XDB–1–5, XDB–1–6 and XDB–1–7) from the Xiaoduobaoshan rock body and monzonitic granite samples (No. WLH–1–8, WLH–1–9 and WLH–1–14) from the Wolihedingzi rock body fall into volcanic arc granite field in the Y–Nb, Yb–Ta, (Yb+Ta)–Rb and (Y+Nb)–Rb diagrams (Fig. 7). Combined with previous data, it can be believed that these rock bodies were formed in a volcanic arc environment.

The northeast China is situated in the easternmost part of the Tianshan–Xingmeng Paleozoic orogen between the North China platform and Siberian platform, and has the features of typical microcontinent. The diagenetic and metallogenic processes are closely related to the evolution of the Paleo–Asian Ocean, Okhotsk Ocean and Palaeo–Pacific Ocean (Maniar and Piccoli, 1989; Ge Wenchun, 2007; Guo Feng et al., 2009; Miao Laicheng et al., 2011; Liu et al., 2012; Bai Ling-an, 2013; Bai Ling-an et al., 2014; Wang et al., 2015; Zhang et al., 2015). According to the Tayuan–Xiguitu, Hegenshan–Heihe, Ximulun–Changchun and Mudanjiang faults, the northeast China is

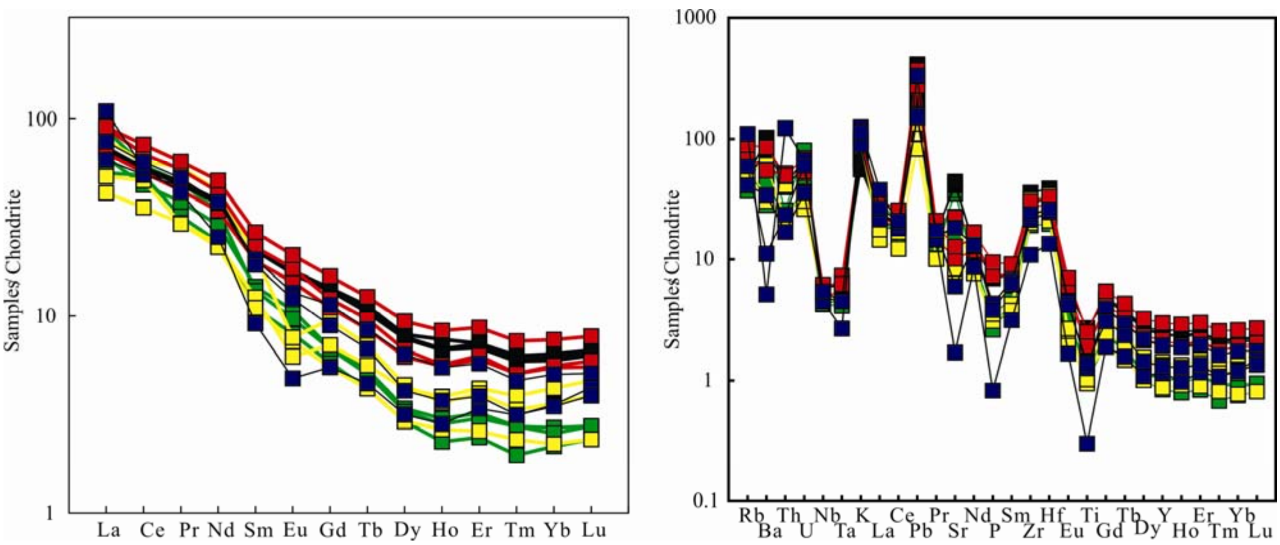

Fig. 6. Rare earth distribution diagram and spider diagram of the trace elements (Sun and McDonough, 1989).

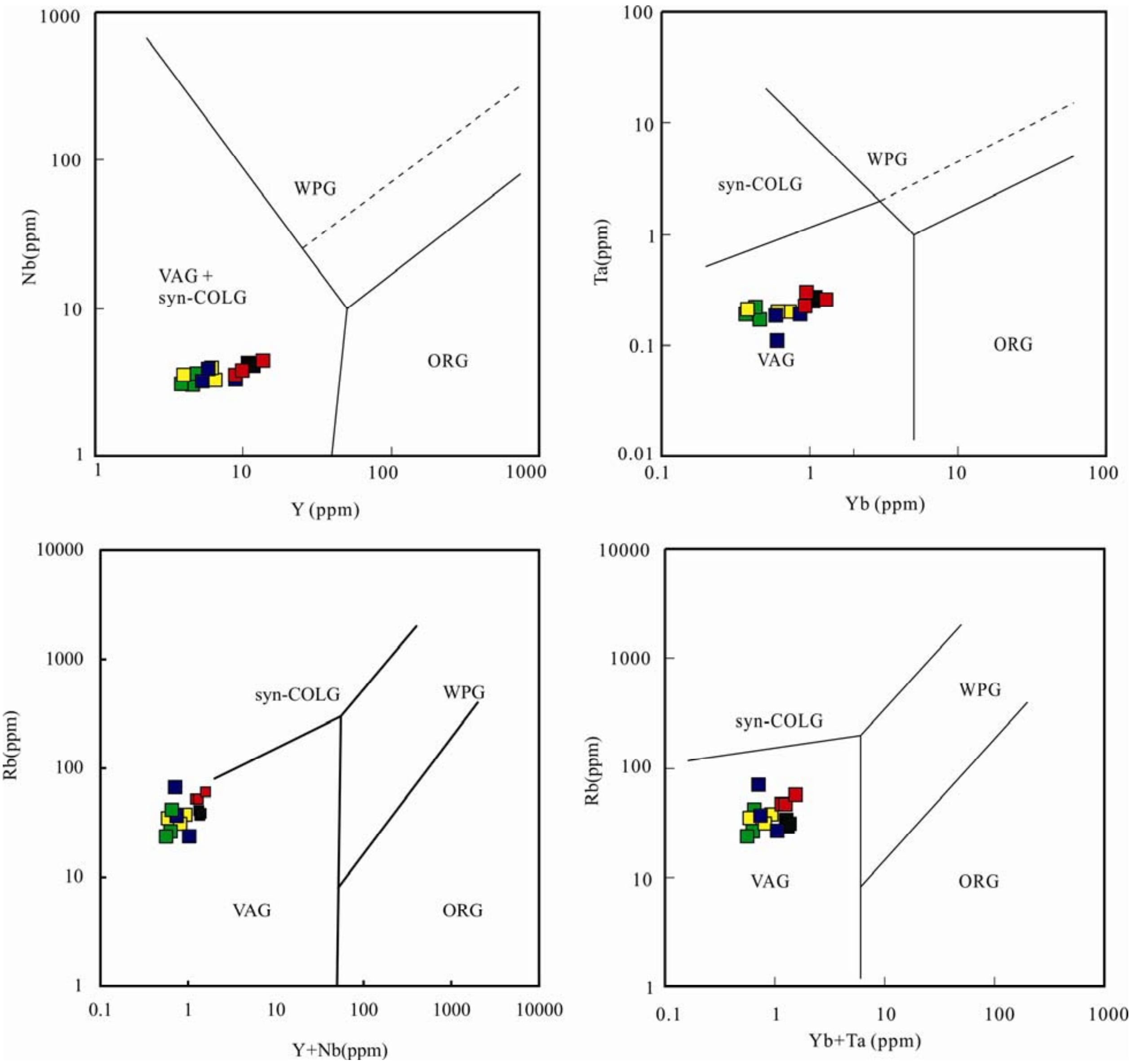

Fig. 7. Y-Nb, Yb-Ta, (Yb+Nb)-Rb and (Yb+Ta)-Rb diagrams.

divided into the Erguna block, Xing'an block and Jiamusi block (Fig. 1a). After Early–Paleozoic, collision and amalgamation occurred between the Jiamusi block and the Songnen block along Jiayin–Mudanjiang area (Zhang Meisheng et al., 1998; Wu Fuyuan et al., 2011), and terminated at the end of Ordovician, forming the Jiamusi–Nenjiang block, while the Erguna block and Xing'an block in the northwest also consitituted the unified Erguna–Xing'an microcontinent in Caledonian. After Middle–Ordovician, collision and amalgamation happened between the Jiamusi–Nenjiang and Erguna–Xing'an microcontinents along Hegenshan–Nenjiang–Heihe area (Li Shuanglin and Ouyang Ziyuan, 1998), and finally formed the Heilongjiang plate solitary between two major plates in Late Devonian to Early Carboniferous, with the Palaeoasian Ocean situated in the south of the plate and the Mongolia–Okhotsk Ocean at its north margin. During Late Permian to Early Triassic, scissors–type collision amalgamation occurred between the North China plate and Heilongjiang plate from west to east along Xilamulun–Changchun–Yanji area (Li Shuanglin and Ouyang Ziyuan, 1998). The Palaeoasian Ocean disappeared, and the Heilongjiang plate became a part of the North China plate, but the Okhotsk Ocean still existed between the Siberian plate and the North China plate (Zhang Meishegn et al., 1998; Li Shuanglin and Ouyang Ziyuan, 1998; Wu et al., 2011). After Late Permian, southward and northward bidirectional subduction of the Okhotsk Ocean happened, scissors-type collision closure of the Mongolian–Okhotsk Ocean occurred, and finally the ocean was closed in Late Jurassic to Early Cretaceous (Zhao et al., 1990;

Kravchinsky et al., 2002), by then, the Siberian plate and the North China plate were sutured together.

In the geological history of China, Mao Jingwen (2012) argued that the Triassic tectonic evolution is characterized by strong intensity and extensive influence. The mineral deposits of Triassic are mainly distributed in the Kunlun–Qinling and Honghe–Ailaoshan Triassic orogenic belts and their adjacent areas. In addition, there are a series of polymetallic minerals in the South China plate, northeast China and Xinjiang, which is consistent with our view that there are Indosinian magmatic activities and mineralization in ore field. A large number of studies have shown that different deposits are often produced in a specific geodynamic setting. Pei Rongfu (2010) considers the deposit to be a specific product of crustal motion, a relic of crustal motion and a very important indicator, which reflects tectonic magmatic thermal events. In this paper, the tectonic setting of the rock mass is volcanic arc, and the diagenetic and metallogenic concentration is 220–230 Ma. Paleomagnetic data show that the Siberian plate was not finally fused with the North China plate until Early Cretaceous (Li Linqing and Ouyang Ziyuan, 1998). Therefore, it is reasonable to conclude that the magmatic activity and metallogenesis of the Indosinian in the study area occurred after the subduction of the north and south of the Okhotsk Oceans: during the beginning of the process of collision orogeny (especially of the metamorphic belt of the two plates), the lithosphere thickened, temperature rose, partial melting appeared in large–scale areas, and magma intruded along the weak part. At last, with the decrease of temperature and pressure, the metal elements gradually released in the favorable areas and uperimposed in the original deposit or formed new deposits.

5.3 Prospecting direction

The Doubaoshan and Tongshan large porphyry Cu–Mo deposits were formed at ~470 Ma in Caledonian (Wang Xicheng et al., 2007; Cui Gen et al., 2008; Xiang Anping et al., 2012; Zhao Huanli et al., 2014). In recent years, the Indosinian rock bodies have been discovered in the Duobaoshan and Tongshan ore districts, with ages of 230.9±2.8 Ma (Zeng Qingdong et al., 2014) and 230−240 Ma (Hao et al., 2015), respectively. The new age of the samples from the Tongshan rock body determined in this study is 223.1±2.8 Ma (Table 3; Fig. 4g and 4h). In addition, the Cu grade in the samples is relatively high, and some samples have been mineralized to ores, with the highest Cu grade up to 0.38wt% (TS–02–6, Table 4). Accordingly, we believe that the Indosinian magmatic activities in the Duobaoshan and Tongshan deposits were overprinted, resulting in further enrichment of the ore–forming materials. The two ages of the granodiorite porphyry from the Xiaoduobaoshan deposit determined in this study are 471.8±7.4 Ma and 222.1±5.5 Ma, respectively (Figs. 4i and 4j; Table 2), indicating that the rock body was formed not only by single magmatic activity. The Xiaoduobaoshan rock bodies (XDB–1–5, XDB–1–6 and XDB–1–7) have similar petrological-geochemical characteristics with the Tongshan granodiorite (Ts02–2, Ts02–5 and Ts02–6) (Figs. 5 and 6; Table 4). In addition, the Xiaoduobaoshan Cu–Mo orebodies occur as small lenses, with average Cu grade of 0.4wt% and average Mo grade of 0.012wt% (Zhao Yuanyi et al., 2011), but the orebodies are small in scale, with the Cu resources of 7,100 t and Mo resources of 154 t (Zhao Yiming et al., 1997b). Therefore, the rock bodies in the Xiaoduobaoshan are the peripheral comprehensive embodiment of the magmatic activities in the Duobaoshan and Tongshan ore districts.

The ages of the Yuejin, 173-kilometer and Wolihedingzi rock bodies are 238.1±2.4 Ma, 238.5±2.1Ma and 238.4±2.0 Ma, respectively, which are highly consistent with each other and exhibit similar petrological-geochemical characteristics (Figs. 5 and 6; Table 4). Thus, they are believed to be formed in the same period of homologous magmatic activity. The ore bodies in the mineralized spots in the Yuejin porphyry Cu–Mo deposit occur as lenses, with average Cu grade of 0.22wt% −0.59wt% and average Mo grade of 0.036wt%−0.072wt% (Yao Zhiqiang et al., 1995). It can be seen that a small amount of mineralization with the characteristics of the root belt of the porphyry copper–molybdenum deposit is produced in the 173-kilometer and Wolihedingzi rock bodies. They can be seen as the beginning of the Indosinian magmatic activities in the Duobaoshan deposit, which last till 200 Ma (Indosinian magmatic activities are also found in Tongshan and Xiaoduobaoshan) and had been accompanied by metallogeneses.

In terms of geographic position and tectonics, under the control of the NW–trending structures, the Yuejin–Duobaoshan–Tongshan structural belt extends northwestwards, and is the major ore–controlling structure in the whole deposit cluster. In addition, the 173-kilometer –Xiaoduobaoshan–Wolihedingzi structural belt also extends northwestwards, nearly parallel to the Yuejin–Duobaoshan–Tongshan structural belt, and in both structural belts some deposits (mineralized bodies) have been discovered, including the Duobaoshan and Tongshan large deposits, Xiaoduobaoshan deposit and Yuejin deposit (spot). Therefore, we suggest giving more support to prospecting in the 173-kilometer–Xiaoduobaoshan–Wolihedingzi area.

6 Conclusions

(1) The ages of the Yuejin monzonitic granite, Tongshan granodiorite, 173-kilometer monzonitic granite, Xiaoduobaoshan granodiorite porphyry and Wolihedingzi monzonitic granite are 238 Ma, 222 Ma, 223 Ma, 238 Ma and 238 Ma, respectively, all belonging to Indosinian.

(2) These rock bodies exhibit consistency in the geochemical characteristics, and all were formed in a volcanic arc environment. The magmatic activity and metallogenesis of the Indosinian in the study area occurred after the subduction of the north and south of the Okhotsk Oceans: during the beginning of the process of collision orogeny (especially of the metamorphic belt of the two plates), the lithosphere thickened, temperature rose, partial melting appeared in large-scale areas, and magma intruded along the weak part. At last, with the decrease of temperature and pressure, the metal elements gradually released in the favorable areas and uperimposed in the original deposit or formed new deposits.

(3) The Yuejin–Duobaoshan–Tongshan and 173-kilometer–Xiaoduobaoshan–Wolihedingzi structural belts both extend northwestwards and are nearly parallel to each other. They are very similar in geotectonic settings and timing of the magmatic activities, and the Indosinian magmatic activities occurred and formed deposits (occurrences) in both of them. We should give more support to porphyry Cu-Mo deposit prospecting in these two metallogenic belts, especially in Yuejin, 173-kilometer and Wolihedingzi areas where less research work has been done.

Acknowledgements

The field work was supported by Senior Engineer Guo Jihai, Senior Engineer Liang Haijun, Senior Engineer Cui Ge, Engineer Tong Kuangyi, Senior Engineer Tang Hui, Senior Engineer Zhu Pengfei, Senior Engineer Qi Yongsheng et al. form the Heilong Mining Go. Limited Ltd. The zircon LA-ICP-MS dating was undertaken at the LA-ICP-MS Office of the Key Laboratory of Crust–Mantle Materials and Environments, University of Science and Technology of China, Chinese Academy of Sciences. The zircon SHRIMP dating was undertaken at Beijing SHRIMP Centre, Chinese Academy of Geological Sciences. The major and trace element analysis was undertaken at the Beijing Research Institute of Uranium Geology. The manuscript was significantly benefited from Professor Xu Bei from the Peking University and Researcher Nie Fengjun from the Chinese Academy of Geological Sciences. We wish to express our sincere thanks to the above institutions and individuals. This research was funded by the National Basic Research Program (973 Program, grant No. 2013CB429805) and the National Key Research and Development Plan (grant No. 2017YFC0601303).

Manuscript received July 1, 2016.
accepted June 9, 2017.
edited by Hao Qingqing

References

Andersen, T., 2002. Correction of common lead in U-Pb analyses that do not report Pb^{204}. *Chemical Geology*, 192(1–2): 59–79.

Bai Ling'an, Sun Jinggui, Gu Alei, Zhao Keqiang and Sun Qinglong, 2014. A review of the genesis, geochronology, and geological significance of hydrothermal copper and associated metals deposits in the Great Xing'an Range, NE China. *Ore Geology Reviews*, 6: 192–203.

Bai Ling'an, 2013. *Metallogenic mechanism and resource prediction of the hydrothermal copper deposit in the middle and north of the Greater Xing'an Mountains*. Changchun: Jilin University (Ph. D thesis): 1–143.

Black, L.P., Kamo, S.L., Allen, C.M., Black, L.P., Kamo, S.L., Allen, C.M., Aleinikoff, J.N., Davis, D.W., Korsch, R. J., and Foudoulisa, C., 2003. TEMORA I: a new zircon standard for Phanerozoic U-Pb geochemistry. *Chemical Geology*, 200: 155–170.

Compston, W., Williams, I.S., and Kirschvink, J.L., 1992. Zircon U-Pb ages for the Early Cambrian time-scale. *Journal of the Geological Society of London* , 149: 171–184.

Cui Gen, Wang Jinyi, Zhang Jingxian and Cui Ge, 2008. U-Pb SHRIMP dating of zircons from Duobaoshan granodiorite in Heilongjiang and its geological significance. *Global Geology*, 27(4): 386–394 (in Chinese with English abstract).

Du Qi, Zhao Yuming, Lu Binggang and Ma Deyou, 1998. *Duobaoshan porphyry copper deposit*. Beijing: Geological Publishing House, 334(in Chinese).

Ge Wenchun, Sui Zhenmin, Wu Fuyuan and Zhang Jiheng, 2007. Zircon U–Pb ages, Hf isotopic characteristics and their significanceof Early Paleozoic granites in the northeastern Hinggan Mts., northeastern China. *Acta Petrologic Sinica*, 23 (2): 423–440 (in Chinese with English abstract).

Guo Feng, Fan Weimin, Li Chaowen, Miao Laicheng and Zhao Liang, 2009. Early Paleozoic subduction of the Paleo–Asian Ocean: Geochronological and geochemical evidence from the Dashizhai basalts, Inner Mongolia. *Science in China Series D Earth Sciences*, 39(5): 569–579(in Chinese with English abstract).

Hao, Y.J., Ren, Y.S., Duan, M.X., Tong, K.Y., Chen, C., Yang, Q., and Li, C., 2015. Metallogenic events and tectonic setting of the Duobaoshan ore field in Heilongjiang Province, NE China. *Journal of Asian Earth Sciences*, (97): 442–458.

Jiang Sihong, Nie Fengjun, Bai Daming, Liu Yifei and Liu Yan, 2011. Geochronology evidence for Indosinian mineralization in Baiyinnuoer Pb-Zn deposit of Inner Mongolia. *Mineral Deposits*, 30(5): 787–798 (in Chinese with English abstract).

Kang Yongjia, She Hongquan, Xiang Pingan, Tian Jing, Li Jinwen, Yang Yuncheng, Guo Zhijun and Dong Xuzhou, 2014. Indo–Chinese magmatic activity in Badaguan ore district and its metallogenic implications. *Geology in China*, 41(4): 1215–1225 (in Chinese with English abstract).

Kravchinsky, V.A., Cogne, J.P., Harbert, W.P., and Kuzmin M.I., 2002. Evolution of the Mongol–Okhotsk ocean as constrained by new paleomagnetic data from the Mongol–Okhotsk suture zone, Siberia. *Geophysical Journal International*, 148: 34–57.

Li Derong, Zhu Chaoli, Lv Jun and Cui Gen, 2010. Structural-magmatic mineralization of the Sankuanggou–Duobaoshan metallogenic belt, Heilongjiang. *China Mining Magazine*, 19 (S1): 142–146 (in Chinese with English abstract).

Li Shuanglin and Ouyang Ziyuan, 1998. Tectonic framework and evolution of Xing'anling–Mongolian orogenic belt (XMOB) and its adjacent region. *Marine Geology and Quaternary Geology*, 18(3): 45–54 (in Chinese with English abstract).

Liu, J., Wu, G., Li, Y., Zhu, M.T., and Zhong, W., 2012. Re-Os sulfide (chalcopyrite, pyrite and molybdenite) systematics and fluid inclusion study of the Duobaoshan porphyry Cu (Mo) deposit, Heilongjiang Province, China. *Journal of Asian Earth Sciences*, 49: 300–312.

Liu Jun, Wu Guang and Zhong Wei, 2010. Fluid inclusion study of the Duobaoshan porphyry Cu (Mo) deposit, Heilongjiang Province, China. *Acta Petrologica Sinica*, 26(5): 1450–1464 (in Chinese with English abstract).

Ludwig, K.R., 2003. *ISOPLOT 3.00: A Geochronological Toolkit for Microsoft Excel*. California: Berkeley Geochronology Center .

Lv Pengrui, Li Derong, Peng Yiwei and Zhang Mingyang, 2012. S-Pb isotopic characteristics of ore sulfides and U-Pb dating of zircon from the Sankuanggou skarn-type Cu–Fe–Mo deposit in Heilongjiang Province. *Geology in China*, 39(03): 717–728 (in Chinese with English abstract).

Maniar, P.D., and Piccoli, P.M., 1989. Tectonic discrimination of granitoids. *Geological Society of America Bulletin*, 101: 635–643.

Mao Jingwen, Zhou Zhenhua, Feng Chengyou, Wang Yitian, Zhang Changqing, Peng Huijuan and Yu Miao, 2012. A preliminary study of the Triassic large-scale mineralization in China and its geodynamic setting. *Geology in China*, 39(6): 1437–1471 (in Chinese with English abstract).

Mao Zhiguo, Zhu Rukai, Luo Jinglan, Wang Jinghong, Du Zhanhai, Su Ling and Zhang Shaomin, 2015. Reservoir characteristics,formation mechanisms and petroleum exploration potential of volcanic rocks in China. *Petroleum Science*, 12: 54–66.

Miao Laicheng, Fan Weiming, Zhang Fuqin, Liu Dunyi, Jian Ping, Shi Guanghai, Tao Hua and Shi Yuruo, 2003. SHRIMP dating of the Xinkailing–Keluo zircon in the northwestern part of the Xiaoxing'an Mountains and its significance. *Chinese Science Bulletin*, 49(22): 2315–2323 (in Chinese with English abstract).

Middlemost, E.A.K., 1994. Naming materials in the magma/igneous rock system. *Earth–Science Reviews*, 37: 215–224.

Pearce, J.A., Harris, N.B.W., and Tindle, A.G., 1984. Trace element discrimination diagrams for the tectonic interpretation of granitic rocks. *Journal of Petrology*, 25(4): 956–983.

Peccerillo, A., and Taylor, S.R., 1976. Geochemistry of Eocene calcalkaline volcanic rocks from the Kastamonu area, northern Turkey. *Contributions to Mineralology and Petrology*, 58: 63–81.

Pei Rongfu, Mei Yanxiong, Wang Yonglei, Zhai Hongyin and Wang Haolin, 2010. The classification of large scale deposit and its metallogenic path trace. *Mineral Deposits*, 29(S1): 20–21 (in Chinese with English abstract).

She Hongquan, Li Jinwen, Xiang Anping, Guan Jidong, Yang Yuncheng, Zhang Dequan, Tan Gang and Zhang Bi, 2012. U-Pb ages of the zircons from primary rocks in middle–northern Daxinganling and its implications to geotectonic evolution. *Acta Petrologica Sinica*, 28(2): 571–594 (in Chinese with English abstract).

Sun, S.S., and McDonough, W.F., 1989. Chemical and isotopic systematics of oceanic basalts: Implications for mantle composition and processes. *Geological Society*, 42: 313–345.

Tang, J., Xu, W.L., Wang, F., Wang, W., Xu, M.J., and Zhang, Y.H., 2014. Geochronology and geochemistry of early–middle Triassic magmatism in the Erguma Massif.Ne China: Constrains on the tectonic evolution of the Mongol–Okhotsk Ocean. *Lithos*, 184–187: 1–16.

Wang Xunlian, Wang Linlian, Liu Jinying, Xia Bin, Chen Jun and Xu Xiumei, 2007. Metallogeny and reformation of the Duobaoshan superlarge porphyry copper deposit in Heilongjiang. *Chinese Journal of Geology*, 42(1): 124–133 (in Chinese with English abstract).

Wang Chao, Li Rongshe, Smithies, R., Hugh., li Meng and Peng Yan, 2015. Felsic magmatic evolution and the role of postcollisional process in continental crustal growth at convergent margins: Insights from the western part of the central Qilian Belt, Northwestern China. *Acta Geologica Sinica* (English Edition), 89(supp. 2): 92–93.

Wei Hao, Xu Jiuhua, Zeng Qingdong, Wang Yanhai, Liu Jianming and Chu Shaoxiong, 2011. Fluid evolution of alteration and mineralization at the Duobaoshan porphyry copper (Mo) deposit, Heilongjiang Province. *Acta Petrologica Sinica*, 27 (5): 1361–1374 (in Chinese with English abstract).

Williams, I.S., 1998. U-Th-Pb geochronology by ion microprobe. In: McKibben, M.A., Shanks, W.C., Ridley, W.I. (Eds.), *Applications of Microanalytical Techniques to Understanding Mineralizing Processes*, Reviews in Economic Geology, 7: 1–35.

Wu, F.Y., Sun, D.Y., Ge, W.C., Zhang, Y.B., Matthew, L., Simon A., and Jahn., 2011. Geochronology of the Phanerozoic granitoids in northeastern China. *Journal of Asian Earth Sciences*, 41(1): 1–30.

Wu Guang, Liu Jun, Zhong Wei, Zhu Mingtian, Mi Mei and Wan Qiu, 2009. Fluid inclusion study of the Tongshan porphyry copper deposit, Heilongjiang Province, China. *Acta Petrologica Sinica*, 25(11): 2995–3006 (in Chinese with English abstract).

Wu Taotao, Chen Cong, Liu Kai, Bao Qingzhong, Zhou Yongheng and Song Wanbing, 2016. Petrogenesis and Tectonic Setting of the Monzonite Granite in Yitulihe area,Northern Great Xing'an Range. *Acta Geologica Sinica*, 90(10): 2637–2647 (in Chinese with English abstract).

Xiang Anping, Yang Yuncheng, Li Guitao, She Hongquan, Guan Jidong, Li Jinwen and Guo Zhijun, 2012. Diagenetic and metallogenic ages of Duobaoshan porphyry Cu-Mo deposit in Heilongjiang Province. *Mineral Deposits*, 31(6): 1237–1248 (in Chinese with English abstract).

Xing Shuwen, Xiao Keyan, Zhang Tong, Tian Fang, Ding Jianhua, Zhang Yong, Ma Lukuo And Ma Yubo, 2016. Geological Characteristics and Mineral Resource Potential of the Cu-Mo-Ag Metallogenic Belt in Daxinganling Mountains. *Geological Review*, 62(7): 1316–1333 (in Chinese with English abstract).

Yao Zhiqiang, Zhang Dequan and Zhao Yuming, 1995. Research on large porphyry copper deposit in Duobaoshan and its adjacent area of Heilongjiang Province. In: *The Third Geological Survey Institute of Heilongjiang Bureau of Geology and Mineral Resources*, 153–251 (in Chinese).

Yang Huaben, Wang Wendong, Yan Yong Sheng, Wei Xiaoyong and Geng Chengbao, 2016. Origin of Basalts of the Tamulangou

Formation and Mantle Enrichment in Xinlin Area, Northern Greater Hinggan Mountains. *Geological Review*, 62(6): 1471–1486 (in Chinese with English abstract).

Yang Yongqiang, Qiu Longwei, Gregg, J., Shi Zheng and Yu Kuanhong, 2016. Formation of fine crystalline dolomites in lacustrine carbonates of the Eocene Sikou Depression, Bohai Bay Basin, East China. *Petroleum Science*, 13: 642–656.

Zeng, Q.D., Liu, Ji.M., Chu, S.X., Wang, Y.B., Sun, Y., Duan, X.X., Zhou, L.L., and Qu, W.J., 2014. Re-Os and U-Pb geochronology of the Duobaoshan porphyry Cu–Mo–(Au) deposit, Northeast China, and its geological significance. *Journal of Asian Earth Sciences*, 79: 895–909.

Zeng Qingdong, Liu Jianming, Zhang Zuolun, Qin Feng, Chen Weijun, Zhang Ruibin, Yu Chang and Ming Yejie, 2009. Ore-forming time of Jiguanshan porphyry molybdnum deposit, northern margin of north China craton and the Indosinian mineralization. *Acta Petrologica Sinica*, 25(2): 393–398 (in Chinese with English abstract).

Zhang Lan, Yang Jingsui and Zhang Jian, 2015. Geochronology and geochemistry of Zengga Mesozoic grantoids from East Gangdese Batholith, Implications for the remelting mechanism of granite formation. *Acta Geologica Sinica* (English Edition), 89(supp. 2): 113–114.

Zhang Lianchang, Wu Huaying, Xiang Peng, Zhang Xiaojing, Chen Zhiguang and Wan bo, 2010. Ore-forming processes and mineralization of complex tectonic system during the Mesozoic: A case from Xilamulun Cu-Mo metallogenic belt. *Acta Petrologica Sinica*, 26(5): 1351–1362 (in Chinese with English abstract).

Zhang Meisheng, Peng Xiangdong and Sun Xiaomeng, 1998. The paleozoic tectonic geographical pattern of northeast China. *Liaoning Geology*, (2): 91–96 (in Chinese with English abstract).

Zhao Guangjiang, Hou Yushu and Wang Baoquan, 2006. Geological characteristics and genisis of Zhengguang gold deposit in Heilongjiang Province. *Non–ferrous Mining and Metallurgy*, 22(3): 3–6 (in Chinese with English abstract).

Zhao Huanli, Zhu Chunyan, Liu Haiyang and Liu Baoshan, 2012. Zircon SHRIMP U-Pb dating and its tectonic implications of the granodiorite in Duobaoshan copper deposit, Heilongjiang Province. *Geology and Resources*, 21(5): 421–424 (in Chinese with English abstract).

Zhao Yiming, Bi Chengsi, Zou Xiaoqiu, Sun Yali, Du Andao and Zhao Yuming, 1997a. The Re-Os isotopic age of molybdenite from Duobaoshan and Tongshan porphyry copper (molybdenum) deposits. *Acta Geoscientia Sinica*, 18(1): 61–67 (in Chinese with English abstract).

Zhao Yiming, Zhang Dequan, Xu Zhigang and Yao Zhiqiang, 1997b. *The metallogenic regularity and prospective evaluation of the copper polymetallic deposit in the Da Xing'an Mountains and its adjacent areas*. Beijing: Seismological Press, 318 (in Chinese).

Zhao Yuanyi and Ma Zhihong, 1997a. A study on ore forming geochemical of Duobaoshan copper deposit, Heilongjiang Province. *Journal of Xi'an College Geology*, 19(1): 28–35 (in Chinese with English abstract).

Zhao Yuanyi, Ma Zhihong and Feng Benzhi, 1997b. *Study on system geochemistry and prospecting of Duobaoshan copper deposit*. Changchun: Jilin People's Publishing House, 155 (in Chinese).

Zhao Yuanyi, Wang Jiangpeng, Zhao Guangjiang and Cui Yubin, 2011. Mineralization regularity and prospecting direction of Duobaoshan ore field, Heilongjiang Province, China. *Journal of Jilin University* (Earth Science Edition), 41(6): 1676–1688 (in Chinese with English abstract).

About the first author

LI Yun, male, born in 1990 in Liuan City, Anhui Province; master; a student of Chinese Academy of Geological Sciences; He is now interested in the study on mineralogy, petrology, mineralogy.E-mail:liyun9012@qq.com.